Xrs2 C-terminus mediates Tel1-dependent meiotic double-strand break interference

Marie Dorme, Rakesh Aithal, Christelle Cayrou, Julien Vernerey, Bertrand Llorente, Valérie Garcia

CRCM, UMR 7258 CNRS, INSERM, Aix Marseille Université, Institut Paoli Calmettes, Marseille, France

Abstract

During meiosis, the programmed formation of DNA double-strand breaks (DSBs) by Spo11, a conserved topoisomerase-like protein, initiates homologous recombination that leads to crossovers between homologous chromosomes, essential for accurate segregation and genome evolution. Because DSBs are a threat to genome integrity, their number, distribution and timing of formation are regulated during the meiotic program. In *S. cerevisiae*, DSB interference prevents the coincident formation of DNA double-strand breaks (DSBs) in neighboring hotspots through a Tel1/ATM dependent mechanism that remains unexplored. Here, we demonstrate that Tel1 is recruited to meiotic DSBs hotspots in response to Spo11-DSB formation. Tel1 also localizes to chromosomal axis sites in a DSB-dependent manner, thus supporting the TLAC model that postulates meiotic DSBs are being formed within the chromosome axis environment. Tel1 recruitment to meiotic DSBs, DSB interference and the meiotic DNA damage checkpoint are dependent on both the Tel1-FATC domain and the C-terminal moiety of Xrs2, known to mediate Tel1-Xrs2 interaction in somatic cells. However, in a Xrs2 (FxF/Y) mutant DSBs interference remains functional despite Tel1 binding to DSB sites being significantly reduced and the Tel1-dependent DNA damage checkpoint abolished. Altogether, this work highlights the complex regulation of Tel1 multiple functions in meiotic cells, and fine-tuning through interaction with Xrs2.

Introduction

During meiosis, the scheduled formation of DSBs by Spo11, a type II topoisomerase, is required for homologous recombination (HR), a process essential for the accurate segregation of homologous chromosomes[1–5]. Meiotic DSBs are concentrated within relatively narrow and non-randomly distributed regions of permissiveness called DSB hotspots (~190 bp wide in *S. cerevisiae* to a few kilobases in mouse) distributed along the genome, that coincide with promoter regions in budding yeast[6–8]. Meiotic DSBs arise concurrently with a structural reorganization of the chromosomes and the development of nucleoproteic axial structures. During this process, the coalescence of axis sites leads to linear arrays of chromatin loops that are anchored at their base along the axial element[9,10]. In *S.cerevisiae*, axis component include the protein Red1, Hop1, and the meiosis-specific kleisin Rec8. While DSBs sites are preferentially located in chromatin loops, HR takes place in the context of the axes, and Spo11-accessory factors essential for DSB formation (Rec114, Mer2 and Mei4) interact with chromosomal axis, suggesting that DSB sites are tethered to axis sites prior DSB formation (the "tethethered loop-axis complex", or "TLAC"[10–12]). A conserved member of the histone H3K4 methyltransferase Set1 complex was proposed to bridge DSB hotspots to chromosome axes: Set1 recognizes H3K4 trimethylation marks around DSB hotspots and interacts with the axis-associated protein Mer2, thus providing a mechanism promoting DSB hotspots interaction with DSB proteins located on the axes[13,14]. The formation of DSBs within the context of chromosomal axes likely provides an optimal environment for inter-homologous recombination repair[11,15].

Because DSBs are precursors of meiotic recombination, their number and position have a direct impact on the distribution of genetic exchanges between parental chromosomes. Importantly, the frequency and position of chromosome breakage is highly regulated and integrated with multiple homeostatic processes that regulate Spo11 activity and shape the recombination distribution over different size scales[16,17]. One such pathway is the negative regulation of DSB formation by the PI3K-related checkpoint kinase Tel1/ATM. In mouse testes from ATM knock-out mice, a ~10 fold increase in DSB numbers has been measured by quantification of SPO11-oligonucleotides[18]. In drosophila and yeast, Tel1 loss also increases DSB formation and recombination[19–23]. Related to the control of DSB formation, Tel1 suppresses the occurrence of multiple DSBs nearby on the same chromatid (over regions up to 70-100kb), a process defined as DSB interference[23]. As a result, the formation of two DSBs at adjacent hotspots (separated by less than ~70kb) occurs less frequently than expected by

chance. In the absence of Tel1, DSB interference is lost, and DSBs can form independently, leading to the formation of measurable "double-cuts" (DCs) by physical analyses. Interestingly, over smaller distances when DSB hotspots are localized within the same chromatin loop, DCs occur in *tel1Δ* at substantially higher frequencies compared to expectation from random. The absence of Tel1 therefore provides a suitable environment for concerted DSBs within chromatin loops[23]. Tel1 function in preventing DSBs formation between adjacent hotspots is conserved in mammals, where the absence of ATM leads to a significant increase in deletions and duplications initiated by double-cuts formed within and between recombination hotspots[24,25].

Altogether these studies show that Tel1/ATM negatively regulates meiotic DSB formation and directly controls the spatial distribution via DSB interference. DSB interference was proposed to be "reactive"[17,23], i.e. DSB dependent, in line with the known function for Tel1 in response to DSB formation in somatic cells. This however has never been demonstrated and the mechanism of meiotic DSB interference remains elusive.

Mutations in ATM causes ataxia telangiectasia (AT), an autosomal recessive inherited disease characterized by a strong predisposition to malignancy, cerebellar degeneration, radiosensitivity, immune deficiencies, premature ageing and sterility[26]. Although ATM implication in various processes is still emerging, abundant mechanistic insight into Tel1/ATM function has been unveiled over the years, and its function in response to DSBs is in particular well characterized. Tel1/ATM is quickly recruited to DSBs in somatic cells to trigger and coordinate -via its kinase activity on a large number of substrates[27]- various complex cellular process such as checkpoint signaling, DNA repair, chromatin remodeling, transcription inhibition and apoptosis[27]. Tel1/ATM also maintains telomere length homeostasis by promoting telomerase recruitment through phosphorylation events[28–30].
Several studies have demonstrated that Tel1/ATM interacts with the C-terminus of Xrs2/Nbs1, a subunit of the Mre11-Rad50-Xrs2/Nbs1 complex that senses and initiates repair of DSBs and short telomeres[31–33]. Yet, the activation of Tel1/ATM by Xrs2/Nbs1 is not fully understood, and the precise relationship between Xrs2-dependent recruitment of Tel1/ATM to DSBs (or telomeres) and the activation of its multiple functions (such as checkpoint control and telomeres maintenance) remains to be clarified[33].

To better understand Tel1 function during meiosis, and in particular the Tel1-dependent mechanism of DSB interference, we examined Tel1 interaction with meiotic chromosomes at specific sites and genome-wide. We demonstrate that Tel1/ATM interacts genome-wide with meiotic DSB hotspots in a Spo11-DSB dependent manner. In agreement with the preferential

binding of Tel1/ATM to blocked DNA ends[34,35], this interaction is stabilized in a *sae2Δ* resection deficient background, where Spo11-bound DSBs accumulate[36]. Tel1 also localizes to chromosomal axis in a Spo11-catalytic dependent manner, indicating that DSB ends interact with axis sites, and further supporting of the TLAC model. Interestingly, whilst the interaction of Tel1 with meiotic DSB hotspots and axis sites is largely dependent on the C-terminus of Xrs2, DSB interference itself remains active in a Xrs2-FXF/Y mutant that significantly reduces Tel1 recruitment to meiotic DSBs. Such observations indicate that a stable or strong association of Tel1 to Spo11-DSBs is not necessary to mediate the process of DSB interference, while being essential for the DNA damage checkpoint induced by unrepaired Spo11-DSBs. Altogether our data highlight the complex regulation of Tel1's multiple functions and how these are fine-tuned through interaction with Xrs2, subunit of the evolutionarily conserved Mre11-Rad50 complex.

Results

Tel1 protein level is increased in a *sae2Δ* background

To explore Tel1 interaction with chromosomes during meiosis, we N-terminally FLAG-tagged Tel1 at the native genomic locus of the *TEL1* gene (Methods). Normal progression in meiosis I and II was observed for FLAG-Tel1 diploid cells as monitored by the appearance of cells with two (MI) or four (MII) nuclei by DAPI staining (Fig.S1a). Interestingly, FLAG-Tel1 protein level increased slightly (~1.5 fold) during meiosis compared to pre-meiotic conditions (t=0) reaching a maximum at 4 h, before decreasing again, thus broadly following kinetics of meiotic DSB formation and repair (Fig.1a,b). However in a *SAE2* defective background where unprocessed DSBs accumulate and a Tel1-dependent checkpoint is activated[37] (Fig. S1a), Tel1 levels increased ~2.5-fold by 4 h, and up to 4-fold by 8 h (Fig. 1a,b). In a *sae2Δ* strain expressing catalytically dead Spo11 (*Spo11Y135F*) where DSBs are not formed, the *sae2Δ*-dependent cell cycle arrest is alleviated (Fig. S1d), and Tel1 protein levels remained similar to wild-type (Fig. 1a,b). Thus, in the *sae2Δ* background, the increase in Tel1 protein level could be a consequence of the accumulation of unresected DSBs, of the activation of the Tel1-dependent DNA damage checkpoint, or both.

To distinguish between these possibilities, we measured Tel1 levels in *DMC1* deficient cells. In this background, meiotic progression is arrested in late meiosis I before its completion (REF + Fig S1d), but DSBs are hyper-resected (REF). From 5 h in meiotic time-courses, Tel1 protein level in the *dmc1Δ* background exceeded its level in wild type, and remained elevated at 8 h. This suggests that cell cycle progression is required for the reduction in Tel1 protein level observed in wild-type cells (Fig.1a,b). However, Tel1 abundance in the *dmc1Δ* did not reach its level measured in the *sae2Δ* background (~1.5-fold versus 2.5-fold at 4 hr, and ~2.5-fold vs

4-fold at 8 h). Thus, in the *sae2Δ* background, both the meiotic prophase arrest and the presence of unresected DSB ends contribute to persistent elevated Tel1 level across meiosis.

Tel1 associates with meiotic hotspots in a DSB dependent manner

Average DSB hotspot activity measured from cell populations varies over several orders of magnitude, the strongest hotspots in *S. cerevisiae* being cleaved in ~15% of the cells[8]. Thus, the detection of protein binding at meiotic DSBs is limited by hotspots frequency of cleavage. In order to determine whether Tel1 interacts with meiotic DSBs, we performed qPCR-based ChIP experiments of FLAG-Tel1 at three "strong" hotspots (*GAT1*, *ATF2* and *ARE1*, respectively ranked by strength 1st, 3rd and 14th within the *S. cerevisiae* genome[8]). While no enrichment of FLAG-Tel1 was detected prior to meiotic DSB formation (time 0 h) at all three DSB hotspots, nor at the control coldspot CDC39 (Fig. 2a,b, Fig. S2a), a subtle (~2-fold) but significant enrichment was detected at all three hotspots 4 h into meiosis, coinciding with the peak in DSB formation (Fig. 2a,b, Fig. S1c, Fig. S2a). No significant enrichment could be detected after 4 h (Fig. 2a), indicating that Tel1 transiently associates with meiotic DSB hotspots, in agreement with the short-lived nature of Spo11-DSBs in a wild-type background.

Because Tel1/ATM was proposed to preferentially bind unresected, protein-bound DSBs[34,35,38], we hypothesized that Tel1 binding to meiotic DSBs might be increased in a *sae2Δ* mutant. In this background Spo11 remains covalently bound to DSB ends due to the abrogation of the Mre11-dependent endonucleolytic pathway that releases Spo11 from 5' DNA ends[36]. Tel1 enrichment at the three hotspots (*GAT1*, *ATF2* and *ARE1*) was detected from 3 h into meiosis, and increased further up to 6 h, consistent with Tel1 preferential binding to unresected DSB ends that accumulates in the *sae2Δ* mutant (Fig. 2c, d, Fig. S2 b, c, d).

While involved in the resection step of meiotic DSB ends[39], Mre11 is also required for DSB formation itself[40], and consistently interacts with DSB hotspots independently of DSB formation[41]. To ask if Tel1 association with DSB hotspots strictly depends on Spo11 cleavage activity, or if (in the same way as Mre11) Tel1 may have functions upstream DSB formation, we tested its chromatin binding in the catalytically dead Spo11 mutant (*Spo11Y135F*). Importantly, Tel1 did not associate to meiotic hotspots in the absence of DSBs (Fig. 2d, Fig. S2d). Thus, Tel1 localizes to meiotic DSB hotspots in a DSB-dependent manner only.

Tel1 binds to meiotic hotpots and axis sites at a genome-wide level

To further investigate Tel1 localization along chromosomes during meiosis, we assessed FLAG-Tel1 binding genome-wide by ChIP-seq in a *sae2Δ* background. As a control we also mapped Spo11-FLAG binding sites, that were previously determined in a wild-type background on four chromosomes by ChIP on chip[42] and genome-wide by ChIP-seq[43]. As for FLAG-Tel1

ChIP-seq, Spo11-FLAG cultures were treated with formaldehyde, thereby detecting not only covalent interactions of Spo11 with unresected DSB sites, but also non-covalent Spo11 interactions[44].

Prior to meiotic entry, FLAG-Tel1 and Spo11-FLAG did not bind to specific regions of chromosomes beside peaks corresponding to "hyper-ChIPable" regions that were common to both, and to the untagged control[45] (Fig S3a). 6h after meiotic entry, when the large majority of DSBs have been formed and remained unrepaired in the *sae2Δ* background[36], Tel1 and Spo11 show discrete ChIPseq signal peaks on all chromosomes (Fig. 3a, Fig. S3b).
To determine whether Tel1 and Spo11 colocalize with DSB sites we compared ChIP-seq signals with DSBs mapped in the *sae2Δ* background by CC-seq[46]. CC-seq enables genome-wide and nucleotide-resolution mapping of DNA breaks in a resection deficient background, where Spo11 remains covalently bound to DSB ends. About 3000 DSBs hotspots were identified by CC-seq genome-wide[46], that spatially and quantitatively correlated with DSBs hotspots identified by Spo11-oligo immunoprecipitation[8,46]. In agreement with Tel1 enrichment to DSB hotspots measured by ChIP-qPCR, Tel1 visually colocalizes with Spo11-FLAG binding sites and DSB peaks generated by CC-seq (Fig. 3b,c , p= 1.66E-17, Fig. S4a,b). Smoothing FLAG-Tel1 signal with windows of increasing size showed alternative domains of higher and lower signal that mirror peaks and valleys previously observed on DSB maps[8,47], and recapitulated by CC-seq (Fig. S4). A second category of Tel1 peaks also colocalizes with the binding sites of Spo11-FLAG but instead alternates with DSB signals and coincides with the binding sites of the meiosis-specific kleisin subunit Rec8[48] (Fig. 3b, d, p=5.26E-14). Thus, Tel1 (with Spo11) also interacts with chromosomal axis regions. To note, Tel1 distribution centered on DSB hotspots is bimodal and normalized signal is higher than at axis sites, while Spo11 normalized signal at DSBs hotspots and axis are similar (Fig. 3c-d, Fig. S4b).

Tel1 and Spo11 ChIP-seq signals correlate well between duplicates (r2=0.9 and 1 respectively, Fig. S5a,b), therefore data were pooled for subsequent finer-scale analyses. Tel1 and Spo11 binding sites were determined with MACS2 and overlapped with each other and with DSB hotspots and axis coordinates (see methods). We defined as axis sites the regions presents in at least two of the Red8, Hop1 and Red1 binding sites (Fig. S5c). We detected 3103 and 3043 peaks of Tel1 and Spo11, respectively (Fig. S5d). Aggregating signals across the genome confirmed a strong correspondence between Tel1, Spo11, DSB hotspots and axis regions, with 81% of Tel1 binding sites overlapping Spo11 binding sites, 59% overlapping with DSB hotspots, and 47% with axis sites (Fig. 3e-g, Fig. S5d-h). Tel1 peaks not colocalizing with either DSB hotspots or axis sites were rare (7%, Fig. 3e), and of lower intensity (P<0.0001, S6a). Conversely, DSB hotspots not associated with Tel1 or Spo11 signal were significantly

weaker (P<0.0001, Fig. S6c). Visual examination showed that those hotspots often overlapped with a Tel1 signal too weak to be identified as such with our peak-calling parameters. Furthermore, the strength of Tel1 —and of Spo11 signals to a lesser extent— correlates strongly with CC-seq signals (R^2=0.8 and 0.7 respectively, $p<2.2e^{-16}$, Fig. 3h,i). At broad scale, Tel1 signal matched DSB suppression zones in telomeric- and centromeric-proximal regions (Fig. 3j,k). Thus, DSB hotspot strength is a major factor determining Tel1 binding level at DSB hotspots, suggesting a constant binding affinity to any DSB. As previously described in a wild-type background[43], the co-occurrence of DSB hotspots and axis sites is relatively rare (fig 3e, Fig. S5g), and DSB hotspots overlapping axis sites are also amongst the weakest (Fig. S6c).

Finally, the correlation between Tel1 and Spo11 peaks at both DSB hotspots and axis sites was highly significant (r2=0.79 and 0.83 respectively, Fig. S5d). Heatmaps centered on DSB hotspots mid-points further confirmed the positive correlation between Tel1 peaks, Spo11 peaks and DSB hotspots strength (Fig. S7a). Spo11 ChIP-seq signal-to-noise in the *sae2Δ* background (at 6h) was largely improved when compared with ChIP-seq experiments performed across time of DSB formation (3h to 5h) in a wild-type background[43] (Fig. S7a). Thus, transient interactions of Spo11 and Tel1 with DSB hotspots are likely enhanced and preserved in the *sae2Δ* background where the HR pathway is halted at the DSB stage.

According to the TLAC model, DSB formation takes place when hotspots sequences present on chromatin loops are tethered to the chromosomal axis, where the RMM (Rec114-Mei4-Mer2) proteins are located[10,12–14] (Fig. 4a). Tel1 presence at the axis sites by ChIPs may therefore be caused by the interaction of DSBs hotspots with the axis regions when DSBs are formed. In order to determine if DSB formation is required for Tel1 localisation to the axis, we performed ChIP-qPCR of FLAG-Tel1 at two axis sites, *GRR1* and *YBP1*, in wild-type, *sae2Δ* and *sae2Δ spo11-Y135F* mutant backgrounds. In the wild type, unlike the transient interaction of FLAG-Tel1 with DSB hotspots (Fig. 2a), no significant enrichment of FLAG-Tel1 to axis sites was detected (Fig. 4b, Fig. S8a). Thus, Tel1 binding to the axis may be too transient and below detection level when resection and repair proceed in the wild-type background. Indeed, Tel1 is enriched by ChIP-qPCR at both axis sites in the *sae2Δ* background (and in agreement with our ChIP-seq data, Fig. 3b,d,g), but its enrichment is reduced compared to DSB hotspots (4 fold vs 7-10 fold, Fig. 4b, Fig. S8a). Importantly, Tel1 binding to axis sites is severely reduced in the absence of DSB formation (*sae2Δ spo11-Y135F* mutant; Fig. 4b, Fig. S8a). We conclude that Tel1 binding to the axis detected by ChIP results from Spo11-DSB formation in the context of the TLAC that brings DSB hotspots, Spo11, Tel1 and the chromosome axis in close proximity.

Xrs2 is required for Tel1 association with meiotic DSBs

The C-terminal region of NBS1 is required to mediate NBS1-ATM interaction and ATM kinase activation[32,49]. In *S. cerevisiae*, Tel1 recruitment to mitotic DSBs and activation of its kinase activity are abolished in a *xrs2-11* mutant, where Xrs2 is truncated for 161 amino-acids at its C-terminus[31] (Fig. 5a). To determine whether Tel1 recruitment to meiotic DSB hotspots requires Xrs2 C-terminal domain, we deleted the corresponding region of *XRS2*. In the *sae2Δ* background, only 50% of the cells progress through the first meiotic division (Fig. 5b). In the *sae2Δ xrs2-11* mutant, similarly to the *sae2Δ tel1Δ,* the cell cycle delay was abrogated and approximately 80% of cells progressed through the first and second meiotic division (Fig. 5b). Thus, in meiotic cells, the DNA-damage checkpoint induced by unprocessed DSBs requires the Xrs2 C-terminal domain, presumably because of its function in mediating Tel1 recruitment to DSBs, itself required for checkpoint activation. To test this hypothesis, we performed ChIP-qPCR of FLAG-Tel1 at *ARE1*, *ATF2* and *GAT1* in the *sae2Δ xrs2-11* mutant. FLAG-Tel1 enrichment was reduced significantly from ~7-fold in the *sae2Δ* control (Fig. 2d) to ~1.5-fold in the *sae2Δ xrs2-11* mutant (Fig. 5c, Fig. S8d). Similarly, FLAG-Tel1 enrichment at the axis sites was abolished in the *sae2Δ xrs2-11* mutant (Fig. S8d). Collectively, these results indicate that Xrs2 C-terminal domain is required for Tel1 recruitment to meiotic DSBs, which is in turn likely essential for the activation of the meiotic DNA damage checkpoint. The reduction of Tel1 enrichment at meiotic DSBs in the *sae2Δ xrs2-11* mutant background could result, at least in part, from the reduced Tel1 protein abundance due to the faster progression into the first meiotic division (Fig. 5b). Indeed, Tel1 levels are reduced ~2 fold at 6 h in the *sae2Δ xrs2-11* background compared to *sae2Δ* (Fig. S9a,b). To prevent precocious cell-cycle progression in the *sae2Δ xrs2-11* background, Tel1 protein level and enrichment at meiotic DSB hotspots by ChIP were measured in a *ndt80Δ* mutant, where the cells arrest in late prophase I in a checkpoint independent manner[50,51]. As expected, the *ndt80Δ sae2Δ xrs2-11* cells did not progress into the first meiotic division (Fig. S9a), and Tel1 protein abundance was restored to its level in the *sae2Δ* (Fig. S9a-c). Importantly, FLAG-Tel1 recruitment was still significantly reduced in the *ndt80Δ sae2Δ xrs2-11* background, indicating that reduced Tel1 protein level in the *sae2Δ xrs2-11* does not indirectly cause reduced binding at DSB hotspots (Fig. S9c,d).

The ATM-binding segment of NBS1 has been narrowed down to a sequence motif termed FxF/Y (residues 740–749) located within its C-terminus[32]. This motif was proposed to be necessary for ATM recruitment to DSBs and activation in mammalian cells[33,49] and xenopus extracts[32]. However, deletion of this motif did not impair the phosphorylation of all ATM substrates, and did not make mice fibroblasts overly sensitive to IR[52], suggesting that this motif is not required for all ATM functions[33]. In *S.cerevisiae*, mutating the corresponding residues

(K846A/F847A) in Xrs2 reduced its interaction with Tel1, but only partially affected telomere length[53]. However, the requirement for those residues in Tel1 recruitment to telomeres or DSBs has not been investigated[53]. We introduced the K846A/F847A mutations at the endogenous Xrs2 locus with and without the N-terminal FLAG-tag and measured cell cycle progression and Tel1 recruitment to meiotic DSB hotspots. Similarly, to *tel1Δ or xrs2-11* cells, the *xrs2-K846A/F847A* mutant abolished the meiotic DNA-damage checkpoint induced by unresected ends in the *sae2Δ* background (Fig. 5b). FLAG-Tel1 recruitment to *ARE1*, *ATF2* and *GAT1* was also significantly reduced in the *sae2Δ xrs2-K846/F847* mutant compared to the *sae2Δ* FLAG-Tel1 control (Fig. 5c; 2 fold vs 6-8 fold), in agreement with these residues being required for Xrs2 interaction with, and recruitment of Tel1 to DSBs.

Tel1 interaction with Xrs2 also requires the C-terminal half of Tel1 FATC domain[54], which is specifically conserved among PIKKs[55]. Deletion of the last nine amino-acids of the FATC domain at the extreme C-terminus of Tel1 was reported to cause defects in both DNA damage response and telomere homeostasis[54]. This truncation also abolishes Tel1 recruitment to HO breaks[54]. We deleted this short stretch of amino-acids to make the *tel1-ΔC* mutant (aa 2778 to 2787, Fig. 5a). Similarly to the *sae2Δ tel1Δ* and *sae2Δ xrs2-11* mutants, the *tel1-ΔC* mutation abolished the delayed nuclear division observed in *sae2*Δ cells (Fig. 5b). Consistently, Tel1 recruitment to meiotic DSB hotspots was significantly reduced in the *FLAG-tel1-ΔC* mutant (Fig. 5c).

Strong Xrs2-dependent Tel1 binding to DSB hotspots is required for activation of the DNA damage checkpoint but not for Tel1-mediated DSB interference

Meiotic DSB interference is controlled by Tel1 and prevents the formation of coincident DSBs on the same molecule[23]. DSB interference can be pleasured by physical analysis: positive interference values indicate DSB interference, values close to zero indicate no DSB interference (i.e. independence), and negative values manifest concerted DSB formation[23]. In the absence of Tel1, coincident DSBs are formed in adjacent hotspots more frequently than if they were occurring independently of each other. For example within the *HIS4::LEU2* locus (sites I and II, Fig. 6a), concerted DSBs lead to ~2.4kb double-cuts (DCs), and negative values of interference[23].

To test if the lack of Xrs2 C-terminus impacts DSB interference, we prepared genomic DNA from *sae2Δ, sae2Δ tel1Δ* and *sae2Δ xrs2-11* mutant meiotic time-courses, and measured frequencies of DSBs at sites I and II within the *HIS4::LEU2* locus (Fig. 6b,d), as well as frequencies of DCs between sites I and II on undigested genomic DNA (Fig. 6c,d). Similarly to the absence of Tel1, the frequency of DCs was significantly elevated in the *sae2Δ xrs2-11*

mutant compared to the *sae2Δ* control (Fig. 6c,d), leading to negative values of DSB interference (Fig. 6e).

Absence of Tel1 was also shown to cause increased coincident cutting and loss of DSB interference between hotspots separated by up to 70-100kb[23] (medium-range interference). To determine if medium-range DSB interference was also lost in the *xrs2-11* mutant, we probed the interval between *leu2::hisG* and *HIS4::LEU2* on chromosome 3. Similarly to the absence of Tel1, DCs were significantly increased in the *xrs2-11* mutant (Fig. S11a,b). Altogether, this suggests that Xrs2-dependent recruitment of Tel1 to Spo11-DSBs is required to mediate DSB interference. Similarly to Tel1-deficient cells or a Xrs2 C-terminal truncation, both DSBs and DCs were increased in the *sae2Δ tel1-ΔC* mutant, leading to negative values of DSB interference (Fig. S10). Thus, the *tel1-ΔC* mutation behaves like a null mutation, conferring defects in both the DNA-damage response and in DSB interference.

Altogether, and at first sight, these findings support the idea that Tel1 recruitment to meiotic DSB hotspots, through its interaction with Xrs2, is required to both mediate DSB interference and activate the meiotic DNA damage checkpoint in response to unresected DNA ends. Surprisingly however, DCs were barely detectable in the *sae2Δ xrsK846A/F847A* mutant (Fig. 6a-d), and DSB interference values were similar to the *sae2Δ* control, where DSB interference is retained (Fig. 6e). Therefore, while mutations in the FxF/Y motif significantly reduce Tel1 recruitment to DSBs hotspots and abolish the Tel1-dependent meiotic DNA damage checkpoint, these residues are not required for Tel1-mediated DSB interference. This unexpected result where Tel1-mediated DSB interference requires a region in Xrs2 C-terminal domain, but not the FXFY motif—a motif that when mutated severely reduces Tel1 binding to DSBs—nuances the simple model where Tel1 recruitment to DSB ends via the Xrs2 C-terminus is required for DSB interference.

Discussion

Tel1/ATM numerous functions and phosphorylation of targets in response to DNA damages, in particular DSBs, have been extensively characterized in the literature. Although Tel1/ATM function was also shown to be required in various aspects of meiotic DSBs responses, no work thus far addressed whether Tel1 is recruited to meiotic Spo11-DSBs hotspots, and if Tel1 recruitment is required for its known meiotic functions, such as DNA damage checkpoint activation in response to meiotic DSB formation and DSB interference.

Tel1 protein level varies during the meiotic cell cycle in a resection and cell cycle progression dependent manner

We first show that steady-state Tel1 protein slightly varies during meiosis, roughly following meiotic DSB formation and repair. We may distinguish 2 phases in the variation of Tel1 protein level: an increase concomitant with the window of DSB formation (from 2 to 4 hr in a wild-type background), followed by a slight decrease when DSBs are repaired (from 4 to 6 hr) and a sharper drop when cells exit meiotic prophase (between 6 and 8 hr). Tel1 level is significantly increased in *sae2Δ* meiotic cells, and our observations indicate that both the accumulation of unresected Spo11-DNA ends and meiotic arrest contribute to steady Tel1 level. To our knowledge an increase in Tel1/ATM protein level in response to DNA damages has not been reported in the literature so far, and may shed light on a novel mode of regulation. Whether this regulation intervenes at a transcriptional or post-transcriptional level, and also occurs in vegetative cells in response to DNA damages -in particular DNA blocking lesions such as trapped topoisomerase II by the action of etoposide- remains to be explored. Tel1 downregulation at later time-point, when cells exit meiotic prophase in the wild-type, may be caused by proteolysis through the 26S proteasome, a major degradation system during meiotic divisions[56].

Detection of Tel1 association with meiotic DSB hotspots is improved in the absence of DSB resection

In order to dissect Tel1 function at meiotic DSBs and in particular in DSB interference, it was fundamental to determine in first instance whether Tel1 binds to meiotic DSB hotspots, and if so, whether Tel1 binding precedes, like Mre11 does[41], or requires DSB formation. In mitotic cells, Tel1 forms foci in response to γ-rays[57] and localizes to HO-induced DSBs through its interaction with the MRX complex[31]. Based on these mitotic properties, Tel1 localisation to meiotic DSBs was likely and anticipated but awaited to be experimentally demonstrated and characterized.

Because Tel1 was previously shown to localise to HO-induced DSBs by ChIP-qPCR, we anticipated being able to detect its binding to meiotic DSBs. However, while the HO DSBs are formed in each cell and accumulates due to lack of repair, during meiosis DSBs are formed at most in ~15% of the cells at the strongest hotspots at a given time, and are immediately resected and repaired. Although we can detect significant enrichment of Tel1 by ChIP-PCR at 4 hrs in meiotic time-courses in a wild-type background at 3 strong hotspots, this enrichment is weak (~1.5 to at 2 fold) and transient, supporting the idea that Tel1 binds to DSB hotspots in response to DSB formation only. As expected, Tel1 enrichment is improved in a *sae2Δ*

background (3-4 fold at 4 hrs, up to ~10 fold at 6 hrs), in agreement with preferential binding of Tel1 to blocked DNA ends that accumulate in this background.

Tel1 associates genome-wide with meiotic hotspots and axis sites in a DSB dependent manner

Using ChIP-seq in the *sae2Δ* background in order to improve detection of Tel1 at meiotic DSBs, we demonstrated that Tel1 binds to DSB hotspots genome-wide, and that binding efficiency correlates with hotspots strength. While Spo11-FLAG also binds to DSB hotspots, its overall signal is weaker than Tel1 (Fig. 3c,d). However, Tel1 and Spo11 ChIP-seq were performed on different meiotic samples, and limitations inherent to ChIP experiments (such as Tel1 and Spo11 likely having different cross-linking efficiencies) hamper sound and absolute quantitative comparisons. In addition, Spo11 covalent binding to DSBs in a *sae2Δ* background may prevents adapters ligation during library preparation, and favor detection of non-covalent interactions. If this is the case however, this will impact similarly both Tel1 and Spo11 ChiP-seq signals detection at meiotic Spo11-DSBs. However, Tel1 bimodal distribution centered on DSB hotspots is likely biologically relevant, reflecting depletion in proximity to the DSB site, while Spo11 normalized signal is focused on the DSB hotspots center (Fig. 3c-d, Fig. S4b), consistent with its role in DSB catalysis.

Meiotic DSB hotspots are located on chromatin loops, with cohesins found at their base on chromosome axes[10]. Several DSB proteins, including Spo11 itself, essentials for DSB formation, are also located on chromosome axes[10,12,42,44], leading to a model where DSB hotspots sequences interact with axis sites prior to DSB formation. This “tethered loop-axis complex” model has been proposed to be important both for controlling DSB formation and for ensuring the interhomolog bias during DSB repair[12,15]. DSB-dependent interaction of Tel1 with axis sites provides further support to the TLAC model and support the hypothesis that broken ends are not immediately released when DSBs are formed. The absence of detectable Tel1 interaction with axis sites in the wild-type background could result from the release of Tel1 from DNA ends when resection initiates, or from limitations in the detection threshold by ChIP, or both. Tel1 localization to the axis sites in response to DSB formation—even transient in a resection proficient background—may be crucial for phosphorylation of various targets, such as Rec114 and Hop1 that are required respectively for downregulation of DSB formation[22] and for the homologous biais[58,59]. It will be of particular interest to determine whether Tel1 interaction with the axis is required for those phosphorylation events. Interestingly, while Tel1 enrichment by ChIP at DSB hotspots is higher than at axis sites, the reverse is observed for Spo11 (Fig. S4b). This is in agreement with Spo11 binding to axis sites independently of DSB

formation[13,42], reinforcing the "platform" model where multiple Spo11 dimers assemble with other pro-DSB factors and catalyzes DSB formation upon loop tethering to the axes sites[60].

Tel1 association with meiotic hotspots and DSB interference requires Xrs2 C-terminal domain

MRX binding to sites of damage precedes Tel1 localization, and Tel1–Xrs2 interaction is required for Tel1 recruitment to DSBs in somatic cells[31,32,49,57]. We showed that Tel1 binding to meiotic DSB hotspots is also dependent on Xrs2 C-terminal region, indicating that Tel1 association to Spo11-DSBs is essential for activation of the meiotic DDR pathway. In agreement with this hypothesis, both the DNA damage meiotic checkpoint and DSB interference are lost in the *xrs2-11* mutant, leading to the proposal that Tel1 recruitment to meiotic DSBs is required for both functions. Moderating this conclusion, the *xrs2-K846/F847* mutant behaves like a null mutation with regard to the meiotic DNA damage checkpoint, and significantly reduce Tel1 recruitment to meiotic DSBs, but does not impact DSB interference. Although surprising and unexpected as DSB interference is proposed (but not demonstrated) to be reactive[17], this mutant was reported to behave almost like a null mutant regarding the DNA damage response in vegetative cells, but to cause only a modest defect in telomeres length homeostasis[53]. Furthermore, Xrs2 interaction with Tel1 was reduced but not completely abolished in the *xrs2-K846/F847* mutant, and Tel1 recruitment to telomeres was not investigated[53], suggesting that residual binding and recruitment of Tel1 may occur and is sufficient for some telomeric functions. In our experiments, Tel1 interaction with DSB hotspots may occur transiently in the *sae2Δ xrs2-K846/F847* mutant, enough to mediate DSB interference, but insufficiently to activate and maintain meiotic DNA damage signaling. This idea is supported by the fact that Tel1 enrichment measured by ChIP in the *sae2Δ xrs2-K846/F847* mutant strain, although significantly reduced compared to the control condition (Fig. 5c), remains detectable and significant among the three hotspots tested. Thus, Tel1 may bind transiently to meiotic DSBs in the *xrs2-K846/F847* mutant, enough for catalytic activities towards specific targets and interference, but insufficiently for activation of the meiotic DNA damage checkpoint. In this scenario, Tel1-Xrs2 interaction through the FxF/Y motif would be necessary to stabilize activated Tel1 at sites of DNA damage, critical for Tel1-mediated DNA damage checkpoint activation, but not for DSB interference. In line with previous work[32] we propose that another FXY motif within the Xrs2 C-terminus may be required for Tel1 full recruitment and activities. To conclude, we propose that Xrs2 interaction with Tel1 at meiotic DSBs modulates Tel1 activation, with different levels of activation being required for various Tel1-dependent processes. While checkpoint activation requires robust DSBs binding (and likely strong kinase activity), DSB interference appears to be less dependent on Tel1 retention to DSBs, and may also rely on kinase independent functions.

DATA ACCESSIBILITY

Raw ChIP-seq libraries are available in the GEO repository under accession number (xxxx)

Figure legends

Figure 1. FLAG-TEL1 protein level varies during meiotic progression, is increased in the absence of resection and in response to prophase arrest.

a, Immunoblot of meiotic TCA extracts at indicated time-points probed with anti-FLAG antibody. Bottom panels: ponceau staining.

b, Quantification of immunoblots (n=3) as per (a). Signal normalisation was performed against ponceau staining before standardisation to time 0h.

Figure 2. Tel1 associates with meiotic hotspots in a DSB dependent manner

a, b. FLAG-Tel1 associates transiently with meiotic hotspots. **a**, FLAG-Tel1 association assessed by ChIP at the ARE1 hotspot relative to the CDC39 control site. Error bars: SD from three independent experiments. **b**, FLAG-Tel1 association assessed by ChIP 4 hr in the meiotic time-courses, at the ARE1, ATF2 and GAT1 hotspots relative to the CDC39 control site. Error bars indicate SD from 6 independent experiments. Corresponding %IP values are plotted in Fig. S2a.

c-d. Tel1 association is increased in a resection defective background (*sae2Δ)*. **c**, FLAG-Tel1 association assessed at the ARE1 hotspot relative to the CDC39 control site at indicated time-points. FE in the wild-type for comparison is from panel **a**. **d**, FLAG-Tel1 association at 6 hr at ARE1, ATF2 and GAT1 hotspots in a *sae2Δ* background is dependent on DSB formation. Error bars indicate SD from 6 independent experiments. %IP values are plotted in Fig. S2 d. FLAG-Tel1 association is measured in a catalytic-null *spo11Y135F* mutant (YF).

Figure 3. Flag-Tel1 localises to meiotic hotspots and axis sites

a, Read coverage of FLAG-Tel1, Spo11-FLAG, DSBs (CC-seq) and Rec8 ChIP-seq on ChrVIII at 6 hr. Horizontal axis: position on the chromosome. Vertical axis: Read coverage for each ChIP-seq subtracted from the input signal. ChIP-seq for Tel1 and Spo11 as well as CC-seq were performed in a *sae2Δ* background. ChIP-seq for Rec8 (GSE69231) was previously performed by Sun X *et al.* in a wild-type background[61].

b, zoom-in on a region of ChrVIII (rectangle on panel **a**) illustrating the overlap of FLAG-Tel1 signal with Spo11-FLAG and Rec8 signals (left grey shaded area), and FLAG-Tel1 signal with Spo11-FLAG and DSB sites (central and right pink shaded areas).

c-d, FLAG-Tel1 (blue) and Spo11-FLAG (orange) read densities (RPKM per 20-bp bins) around ±5 kb from DSBs (c) and axis (d) peak centers, identified respectively by CC-seq[46], and by the intersect of Rec8, Red1 and Hop1 ChIP seq (Fig. S5c)[61].

e, Table of overlap between axis, DSBs, Tel1 and Spo11 peaks relative to each other's. Percentages are indicated for the features in the first line relative to features in the first column. "Alone" in the bottom line refers to peaks overlapping with none of the other features.

f, g, Venn diagrams showing the overlap between the number of ChIP–seq (Spo11, Tel1 and Axis) or CC-seq (DSBs) peaks identified for the indicated features.

h, i, Correlation plot between Tel1 signals (h), Spo11 (i), and DSB signals (measured by CC-seq). CPM: counts per millions mapped reads; HPM: hits per million mapped reads.

j, **k**. Telomere-proximal and pericentric Tel1 signal suppression. Points are count densities in 500bp segments averaged across all 32 chromosomes arms. Trend line is indicated by a blue line. Dashed black line shows total reads genome average.

Figure 4. Flag-Tel1 localisation to axis sites is dependent on DSB formation

a, the tethered loop-axis model for DSB formation ('TLAC'). DSB formation occurs when DSB hotspots (localised in chromatin loops) are tethered to axis sites[10–12].

b, FLAG-Tel1 associates with axis sites in a DSB-dependent manner. FLAG-Tel1 association in a *sae2Δ SPO11* and *sae2Δ spo11-Y135F* mutant assessed by ChIP at GRR1 and YBP1 axis sites relative to the CDC39 control site. Error bars indicate SD from 3 independent experiments. %IP values are plotted in Fig. S8a.

Figure 5. Tel1 association to meiotic DSBs is dependent on Xrs2 C-terminal domain

a, Schematic representation of Tel1, Xrs2 and mutants generated in this study: *xrs2-11*, *xrs2-K846A/F847A* and *tel1-ΔC*. The HEAT (Huntington's elongation factor 3, a subunit of protein phosphatase 2A, TOR1) repeats, FAT (FRAP/ATM/TRRAP) domain, FATC (FAT C-terminal) domain of Tel1 and FHA (forkhead-associated), MID (Mre11 interaction) and TID (Tel1 interaction) domains of Xrs2, are indicated.

b, Meiotic cell cycle progression inferred by the percentage of cells with 2 (MI) or 4(MII) nuclei at indicated times after entering meiosis. About 200 cells were scored by DAPI staining for each time point.

c, FLAG-Tel1 association measured by ChIP at the ARE1, ATF2 and GAT1 hotspots relative to the CDC39 control site. Error bars indicate SD from 4 (*xrs2-11*), 6 (*xrs2-K846A/F847A*) and 3 (*tel1-ΔC*) independent experiments. %IP values are plotted in Fig. S8b. *sae2Δ* control values are from Fig. 2d.

Figure 6. DSB interference is abolished in *xrs2-11*, but not in the *xrs2-KF* mutant.

a, Diagram of *HIS4::LEU2* locus showing DSB sites I and II positions, fragment sizes and probes for assaying DSBs and double-cuts (DCs) frequencies.
b, **c**, PstI-digested (**b**) or undigested (**c**) genomic DNA isolated from the indicated time-points after induction of meiosis was fractionated by electrophoresis, transferred to nylon membrane and hybridized with probes as indicated (Right probe: *MRX2*, Central probe: *LEU2*). P, PstI-digested parental DNA; U, uncut parental DNA. DSB signals are marked with open triangles. Double-cuts: DCs. Parts of a unique membrane were cropped for presentation purpose.
d, Quantification of DSBs and double-cuts (DCs) signal in b,c (n=3, mean +-SEM).
e, Interference values $I=1-(DC_{obs}/DC_{exp})$.

Supplementary Figure legends

Figure S1.
a, Meiotic cell cycle progression as the percentage of cells with 2 (MI) or 4(MII) nuclei at indicated times after entering meiosis. About 200 cells were scored by DAPI staining for each time point.
b, Meiotic cell cycle progression as the percentage of cells with 2 (MI) or 4(MII) nuclei at indicated times after entering meiosis. About 200 cells were scored by DAPI staining for each time point. Experimental samples correspond to Fig. 1.

Figure S2
a, %IP values corresponding to Figure 2b (n=6)
b,**c** %IP and fold enrichment of FLAG-Tel1 at different timepoints after entry into meiosis (SPM), at the indicated hotspots (ARE1, ATF2, GAT1) and control site (CDC39). The fold enrichment at ARE1 hotspot is also plotted on Fig. 2c.
d, %IP values of FLAG-Tel1 at 6 hrs into meiosis in *SPO11* and *spo11-Y135F* (n=6 and n=3 respectively), corresponding to Fig. 2d.

Figure S3
a, Pre-meiotic ("high-chippable") FLAG-Tel1, Spo11-FLAG ChIP signal in a *sae2Δ* background. Note that a similar signal is observed in the untagged *sae2Δ* control strain. This signal was substracted for data analyses (see materiels and methods).
b, FLAG-Tel1 (blue) and Spo11-FLAG (yellow) ChIP signal in a *sae2Δ* background on each chromosome of *S. cerevisiae*. Signals are smoothed with a 25kb sliding Hann window. The position of the centromeres is indicated with the black circle on the horizontal axis.

Figure S4

a, Spatial and quantitative agreement of Tel1 signal (upper panels) with DSB signal determined by CC-seq (lower panels). The ChIP-seq profile is shown as an example on Chr3, but Tel1 and CC-seq signals agree well on all chromosomes. The position of the centromere is indicated with the black circle on the horizontal axis. Signal values are plotted after smoothing with an increasing sliding Hann window size as indicated.
b, FLAG-Tel1 and Spo11-FLAG read profiles relative to DSBs and axis peak centers, identified respectively by CC-seq, and by the intersect of Rec8, Red1 and Hop1 ChIP seq.

Figure S5
a,**b** Correlation between biological replicates. Tel1 and Spo11 reads were counted on "between-replicates" merged peak sets using featureCounts. Coefficient of determination (R^2) and associated p-value were determined using linear model fitting function (*lm*).
c, Venn diagrams showing the association between Hop1, Rec8 and Red1 peak coordinates[61]. We define axis coordinates as the intersection of at least two of the three marks (Fig. 3e-g). Overlap percentages are indicated in the table below.
d, Table of overlap between axis, DSBs, Tel1 and Spo11 peaks relative to each other's. Numbers of identified peaks are indicated for the features in the first line relative to features in the first column. "Alone" in the bottom line refers to non-overlapping peaks with any features.
e-h, Overlap between axis, DSBs and Tel1 peaks. Boxplot of comparison between real and shuffled distribution of Tel1 (e,g) or DSBs (f,h) peaks along the genome for the overlap with the indicated features. Ten independent random genomic region shuffling were generated. Center, lower edge, and upper edge of the boxplot denote median, 25th, and 75th percentiles; lower end and higher end of the vertical lines denote 5th and 95th percentiles. Mann Whitney test p-values are indicated.

Figure S6
a-c Boxplot of the Tel1, Spo11 and DSBs peak strength distribution. Tel1 and Spo11 peak strength was quantified by RPKM (Reads per kilobases per million reads). DSBs peak strength was quantified by NormHpM (bioRxiv 10.1101/2023.03.20.533494). The solid horizontal line represents the median, and the box encompasses the lower and upper quartiles. The vertical lines denote 5th and 95th percentiles. Mann Whitney test p-values are indicated.
a, Tel1 peaks are split according to their overlap with Spo11, DSBs, axis, or with none of the above ('alone'). Tel1 peaks not associated with other features (Spo11, DSBs or axis sites) are highly significantly weaker than all the others.

b, Spo11 peaks are split according to their overlap with Tel1, DSBs, axis, or with none of the above ('alone'). Spo11 peaks not associated with other features (Tel1, DSBs or axis sites) are highly significantly weaker than all the others.
c, DSBs peaks are split according to their overlap with Tel1, Spo11, axis, or with none of the above ('alone'). DSBs peaks not associated with other features (Tel1, Spo11 or axis sites) are highly significantly weaker than all the others.
d, Scatterplot in log scale of Tel1 RPM coverage versus Spo11 RPM coverage on Tel1 peaks. RPM/peak were divided by the peak length. All Tel1 peaks (right panels) are split according to their overlap with DSBs (left panels) or axis sites (middle panels). Tel1 ChIP-seq coverage at 6 h in SPM was compared to Spo11 ChIP-seq coverage at 0 h (first line and grey circles on the bottom line) or at 6 h in SPM (second line and black circle on the bottom line). Scatterplots on the bottom line represent the overlay of the scatterplots on the two first lines.

Figure S7
a-b Heatmap of the CC-seq and ChIP-seq read densities of the indicated features around ±5 kb from DSBs center peaks (**a**) or axis sites center (**b**). Regions are ordered according to DSBs strength (NormHpM) in all heatmaps presented in (**a**) or according to Hop1 ChIP-seq signal[61] (RPKM) in all heatmaps presented in (**b**).

Figure S8
a, %IP values of FLAG-Tel1 at 6 hrs into meiosis in *sae2Δ SPO11* and *sae2Δ spo11-Y135F* mutant (n=3), corresponding to Fig. 4b.
b, %IP values of FLAG-Tel1 at 6 hrs into meiosis in *xrs2-11* (n=4), *xrs2-K846A/F847A* (n=6) and *tel1-ΔC* (n=3), corresponding to Fig. 5c.

Figure S9.
Reduced FLAG-Tel1 binding to meiotic hotspots in the *xrs2-11 sae2Δ* background is not caused by reduced Tel1 protein level
a, Meiotic progression assessed by DAPI staining. About 200 cells were scored for each time point.
b, Meiotic protein extracts at the indicated time were examined for FLAG-Tel1 protein level by western-blotting with an anti-FLAG antibody. Lower panel: blotting with an Hsp104 antibody for loading control.
c, Quantification of immunoblots (n=2) for Tel1 level as per (a). Tel1 signal is normalised with Hsp104 signal relative to 0 hr.
d,**e** FLAG-Tel1 association by ChIP at the ARE1 hotspot relative to the CDC39 control site. Error bars indicate SD from two independent experiments. d, Fold enrichment. e, %IP.

Figure S10. Tel1 association to meiotic DSBs, DSB interference and the meiotic DNA damage checkpoint are dependent on Tel1 C-terminal extremity. The *tel1-ΔC* mutation introduces a termination codon at the amino acid residue 2778, removing the amino acids 2778 to 2787.
a, **b**, PstI-digested (**a**) or undigested (**b**) genomic DNA isolated from the indicated time points after induction of meiosis was fractionated by electrophoresis, transferred to nylon membrane and hybridized with probes as indicated (Right probe: *MRX2*, Central probe: *LEU2*). P, PstI-digested parental DNA; U, uncut parental DNA. DSB signals are marked with open triangles. Samples are parts of the same membrane that was cropped for presentation purpose.
c, Quantification of DSBs and double-cut signals in a,b
d, Interference values $I=1-(DC_{obs}/DC_{exp})$.

Figure S11. Middle-range DSB interference is abolished in the *xrs2-11* mutant.
a, Genomic DNA isolated from the indicated time points after induction of meiosis was prepared in plugs and fractionated by PFGE, transferred to nylon membrane and hybridized with a *FRM2* probe located between the *HIS4::LEU2* and *leu2::hisG* hotspots on the left arm of chromosome III. U, uncut parental DNA. Major double-cut signal is indicated by an asterisk.
b, Quantification of observed double-cut signals in a (n=3, mean +-SEM).

References

1. Sun, H., Treco, D., Schultes, N. P. & Szostak, J. W. Double-strand breaks at an initiation site for meiotic gene conversion. *Nature* **338**, 87–90 (1989).
2. Cao, L., Alani, E. & Kleckner, N. A pathway for generation and processing of double-strand breaks during meiotic recombination in S. cerevisiae. *Cell* **61**, 1089–1101 (1990).
3. Bergerat, A. *et al.* An atypical topoisomerase II from Archaea with implications for meiotic recombination. *Nature* **386**, 414–417 (1997).
4. Keeney, S., Giroux, C. N. & Kleckner, N. Meiosis-specific DNA double-strand breaks are catalyzed by Spo11, a member of a widely conserved protein family. *Cell* **88**, 375–384 (1997).
5. Yadav, V. K. & Claeys Bouuaert, C. Mechanism and Control of Meiotic DNA Double-Strand Break Formation in S. cerevisiae. *Front. Cell Dev. Biol.* **9**, 642737 (2021).

6. Petes, T. D. Meiotic recombination hot spots and cold spots. *Nat. Rev. Genet.* **2**, 360–369 (2001).
7. Lichten, M. Meiotic Chromatin: The Substrate for Recombination Initiation. in *Recombination and Meiosis: Models, Means, and Evolution* (eds. Egel, R. & Lankenau, D.-H.) 165–193 (Springer, 2008). doi:10.1007/7050_2008_040.
8. Pan, J. *et al.* A hierarchical combination of factors shapes the genome-wide topography of yeast meiotic recombination initiation. *Cell* **144**, 719–731 (2011).
9. Zickler, D. & Kleckner, N. Meiotic chromosomes: integrating structure and function. *Annu. Rev. Genet.* **33**, 603–754 (1999).
10. Blat, Y., Protacio, R. U., Hunter, N. & Kleckner, N. Physical and functional interactions among basic chromosome organizational features govern early steps of meiotic chiasma formation. *Cell* **111**, 791–802 (2002).
11. Kleckner, N. Chiasma formation: chromatin/axis interplay and the role(s) of the synaptonemal complex. *Chromosoma* **115**, 175–194 (2006).
12. Panizza, S. *et al.* Spo11-accessory proteins link double-strand break sites to the chromosome axis in early meiotic recombination. *Cell* **146**, 372–383 (2011).
13. Sommermeyer, V., Béneut, C., Chaplais, E., Serrentino, M. E. & Borde, V. Spp1, a member of the Set1 Complex, promotes meiotic DSB formation in promoters by tethering histone H3K4 methylation sites to chromosome axes. *Mol. Cell* **49**, 43–54 (2013).
14. Acquaviva, L. *et al.* The COMPASS subunit Spp1 links histone methylation to initiation of meiotic recombination. *Science* **339**, 215–218 (2013).
15. Kim, K. P. *et al.* Sister cohesion and structural axis components mediate homolog bias of meiotic recombination. *Cell* **143**, 924–937 (2010).
16. Keeney, S., Lange, J. & Mohibullah, N. Self-organization of meiotic recombination initiation: general principles and molecular pathways. *Annu. Rev. Genet.* **48**, 187–214 (2014).
17. Cooper, T. J., Garcia, V. & Neale, M. J. Meiotic DSB patterning: A multifaceted process. *Cell Cycle Georget. Tex* **15**, 13–21 (2016).

18. Lange, J. *et al.* ATM controls meiotic double-strand-break formation. *Nature* **479**, 237–240 (2011).
19. Zhang, L., Ma, H. & Pugh, B. F. Stable and dynamic nucleosome states during a meiotic developmental process. *Genome Res.* **21**, 875–884 (2011).
20. Joyce, E. F. *et al.* Drosophila ATM and ATR have distinct activities in the regulation of meiotic DNA damage and repair. *J. Cell Biol.* **195**, 359–367 (2011).
21. Anderson, C. M., Oke, A., Yam, P., Zhuge, T. & Fung, J. C. Reduced Crossover Interference and Increased ZMM-Independent Recombination in the Absence of Tel1/ATM. *PLoS Genet.* **11**, e1005478 (2015).
22. Carballo, J. A. *et al.* Budding yeast ATM/ATR control meiotic double-strand break (DSB) levels by down-regulating Rec114, an essential component of the DSB-machinery. *PLoS Genet.* **9**, e1003545 (2013).
23. Garcia, V., Gray, S., Allison, R. M., Cooper, T. J. & Neale, M. J. Tel1(ATM)-mediated interference suppresses clustered meiotic double-strand-break formation. *Nature* (2015).
24. Lukaszewicz, A., Lange, J., Keeney, S. & Jasin, M. De novo deletions and duplications at recombination hotspots in mouse germlines. *Cell* **184**, 5970-5984.e18 (2021).
25. Lukaszewicz, A., Lange, J., Keeney, S. & Jasin, M. Control of meiotic double-strand-break formation by ATM: local and global views. *Cell Cycle Georget. Tex* **17**, 1155–1172 (2018).
26. Savitsky, K. *et al.* A single ataxia telangiectasia gene with a product similar to PI-3 kinase. *Science* **268**, 1749–1753 (1995).
27. Matsuoka, S. *et al.* ATM and ATR substrate analysis reveals extensive protein networks responsive to DNA damage. *Science* **316**, 1160–1166 (2007).
28. Colombo, C. V., Gnugnoli, M., Gobbini, E. & Longhese, M. P. How do cells sense DNA lesions? *Biochem. Soc. Trans.* **48**, 677–691 (2020).
29. Greenwell, P. W. *et al.* TEL1, a gene involved in controlling telomere length in S. cerevisiae, is homologous to the human ataxia telangiectasia gene. *Cell* **82**, 823–829 (1995).

30. Di Domenico, E. G., Romano, E., Del Porto, P. & Ascenzioni, F. Multifunctional role of ATM/Tel1 kinase in genome stability: from the DNA damage response to telomere maintenance. *BioMed Res. Int.* **2014**, 787404 (2014).
31. Nakada, D., Matsumoto, K. & Sugimoto, K. ATM-related Tel1 associates with double-strand breaks through an Xrs2-dependent mechanism. *Genes Dev.* **17**, 1957–1962 (2003).
32. You, Z., Chahwan, C., Bailis, J., Hunter, T. & Russell, P. ATM Activation and Its Recruitment to Damaged DNA Require Binding to the C Terminus of Nbs1. *Mol. Cell. Biol.* **25**, 5363–5379 (2005).
33. Syed, A. & Tainer, J. A. The MRE11-RAD50-NBS1 Complex Conducts the Orchestration of Damage Signaling and Outcomes to Stress in DNA Replication and Repair. *Annu. Rev. Biochem.* **87**, 263–294 (2018).
34. Fukunaga, K., Kwon, Y., Sung, P. & Sugimoto, K. Activation of protein kinase Tel1 through recognition of protein-bound DNA ends. *Mol. Cell. Biol.* **31**, 1959–1971 (2011).
35. Álvarez-Quilón, A. *et al.* ATM specifically mediates repair of double-strand breaks with blocked DNA ends. *Nat. Commun.* **5**, 3347 (2014).
36. Neale, M. J., Pan, J. & Keeney, S. Endonucleolytic processing of covalent protein-linked DNA double-strand breaks. *Nature* **436**, 1053–1057 (2005).
37. Usui, T., Ogawa, H. & Petrini, J. H. A DNA damage response pathway controlled by Tel1 and the Mre11 complex. *Mol. Cell* **7**, 1255–1266 (2001).
38. Yu, T.-Y., Kimble, M. T. & Symington, L. S. Sae2 antagonizes Rad9 accumulation at DNA double-strand breaks to attenuate checkpoint signaling and facilitate end resection. *Proc. Natl. Acad. Sci. U. S. A.* **115**, E11961–E11969 (2018).
39. Tsubouchi, H. & Ogawa, H. A novel mre11 mutation impairs processing of double-strand breaks of DNA during both mitosis and meiosis. *Mol. Cell. Biol.* **18**, 260–268 (1998).
40. Johzuka, K. & Ogawa, H. Interaction of Mre11 and Rad50: two proteins required for DNA repair and meiosis-specific double-strand break formation in Saccharomyces cerevisiae. *Genetics* **139**, 1521–1532 (1995).

41. Borde, V. *et al.* Association of Mre11p with double-strand break sites during yeast meiosis. *Mol. Cell* **13**, 389–401 (2004).
42. Kugou, K. *et al.* Rec8 guides canonical Spo11 distribution along yeast meiotic chromosomes. *Mol. Biol. Cell* **20**, 3064–3076 (2009).
43. Ito, M. *et al.* Meiotic recombination cold spots in chromosomal cohesion sites. *Genes Cells Devoted Mol. Cell. Mech.* **19**, 359–373 (2014).
44. Prieler, S., Penkner, A., Borde, V. & Klein, F. The control of Spo11's interaction with meiotic recombination hotspots. *Genes Dev.* **19**, 255–269 (2005).
45. Teytelman, L., Thurtle, D. M., Rine, J. & van Oudenaarden, A. Highly expressed loci are vulnerable to misleading ChIP localization of multiple unrelated proteins. *Proc. Natl. Acad. Sci. U. S. A.* **110**, 18602–18607 (2013).
46. Gittens, W. H. *et al.* A nucleotide resolution map of Top2-linked DNA breaks in the yeast and human genome. *Nat. Commun.* **10**, 4846 (2019).
47. Baudat, F. & Nicolas, A. Clustering of meiotic double-strand breaks on yeast chromosome III. *Proc. Natl. Acad. Sci. U. S. A.* **94**, 5213–5218 (1997).
48. Klein, F. *et al.* A central role for cohesins in sister chromatid cohesion, formation of axial elements, and recombination during yeast meiosis. *Cell* **98**, 91–103 (1999).
49. Falck, J., Coates, J. & Jackson, S. P. Conserved modes of recruitment of ATM, ATR and DNA-PKcs to sites of DNA damage. *Nature* **434**, 605–611 (2005).
50. Xu, L., Ajimura, M., Padmore, R., Klein, C. & Kleckner, N. NDT80, a meiosis-specific gene required for exit from pachytene in Saccharomyces cerevisiae. *Mol. Cell. Biol.* **15**, 6572–6581 (1995).
51. Chu, S. & Herskowitz, I. Gametogenesis in yeast is regulated by a transcriptional cascade dependent on Ndt80. *Mol. Cell* **1**, 685–696 (1998).
52. Stracker, T. H., Morales, M., Couto, S. S., Hussein, H. & Petrini, J. H. J. The carboxy terminus of NBS1 is required for induction of apoptosis by the MRE11 complex. *Nature* **447**, 218–221 (2007).

53. Ma, Y. & Greider, C. W. Kinase-independent functions of TEL1 in telomere maintenance. *Mol. Cell. Biol.* **29**, 5193–5202 (2009).

54. Ogi, H. *et al.* Requirement of the FATC domain of protein kinase Tel1 for localization to DNA ends and target protein recognition. *Mol. Biol. Cell* **26**, 3480–3488 (2015).

55. Bosotti, R., Isacchi, A. & Sonnhammer, E. L. FAT: a novel domain in PIK-related kinases. *Trends Biochem. Sci.* **25**, 225–227 (2000).

56. Wen, F. *et al.* Distinct temporal requirements for autophagy and the proteasome in yeast meiosis. *Autophagy* **12**, 671–688 (2016).

57. Lisby, M., Barlow, J. H., Burgess, R. C. & Rothstein, R. Choreography of the DNA damage response: spatiotemporal relationships among checkpoint and repair proteins. *Cell* **118**, 699–713 (2004).

58. Ho, H.-C. & Burgess, S. M. Pch2 acts through Xrs2 and Tel1/ATM to modulate interhomolog bias and checkpoint function during meiosis. *PLoS Genet.* **7**, e1002351 (2011).

59. Carballo, J. A., Johnson, A. L., Sedgwick, S. G. & Cha, R. S. Phosphorylation of the axial element protein Hop1 by Mec1/Tel1 ensures meiotic interhomolog recombination. *Cell* **132**, 758–770 (2008).

60. Johnson, D. *et al.* Concerted cutting by Spo11 illuminates meiotic DNA break mechanics. *Nature* **594**, 572–576 (2021).

61. Sun, X. *et al.* Transcription dynamically patterns the meiotic chromosome-axis interface. *eLife* **4**, (2015).

METHODS

Strains and media

All *S.cerevisiae* strains used in this study are derivatives of the SK1 diploid used for its efficient meiotic entry and progression. Strain genotypes are listed in Table S1.
To generate the FLAG-tag SK1 strain, a URA3 cassette was integrated upstream the Tel1 promoter. The 5' region of *3xFLAG-TEL1* from the FLAG-Tel1 strain generated by Seidel *et al.* (Seidel *et al.* 2008) was amplified by PCR and transformed in the *URA3-TEL1* SK1 strain. After selection on 5-FOA plates, the FLAG-tag insertion was verified by PCR screening and sequencing.
Strains with deletion and mutations were constructed by one-step allele replacement. The *xrs2-11*::*kanMX6, xrs2-KF::KANMX6 and tel1ΔC::KANMX6* strains were made by transformation of a fusion PCR product generated using pFA6a-kanMX6 as a template and 500bp homology fragments. Oligonucleotides are listed in table S2.

Meiotic Time courses

Pre-culture of 8 – 10 colonies were performed in YPD + AU (Yeast Extract 1%, Peptone 2%, Glucose 2%, Adenine and Uracil 0.0137%) for 30h at 30°C, 210rpm agitation. 0.2 OD/ml of cells were incubated in 200ml pre-sporulation medium (SPS: Yeast Extract 0.5%, Peptone 1%, Yeast Nitrogen Base 0.17%, Potassium Acetate 1%, Ammonium Sulphate 0.5%, Potassium Hydrogen Phtalate 0.05M, Antifoam 0.001%) for 14h at 30°C with 250rpm agitation. Cells were collected and washed with water, before incubation at 30°C with 250rpm agitation in pre-warmed sporulation medium (SPM: 1% Potassium Acetate, Antifoam 0.001%). Sample were collected at different time point and treated accordingly to the following experiments.

Meiotic Progression

50µl of cells were collected at different time-points and fixed in ethanol 70%. Meiotic progression was monitored by DAPI staining and counting nuclei content by fluorescence microscopy. ~200cells were counted for each condition.

Chromatin immunoprecipitation (ChIP)

For each meiotic time point, 2 x 10^8 cells were fixed in paraformaldehyde (1% final). FLAG-Tel1 cells were fixed for 30min, while FLAG-Spo11 strain were fixed in for 15min, quenched by glycine for 5min (125mM final) and washed in TBS 1X two times. Cells were lysed using mechanical lysis (Fastprep, 4 cycles at 6.5M/sec 30sec) together with a Lysis buffer (50mM HEPES-KOH, 140mM NaCl, 1mM EDTA pH8, 1% Triton X100, 0.1% Sodium Deoxycholate) complemented with protease inhibitor cocktail tablet (Roche, Ref 05 892 791 001), PMSF (1mM final), pepstatin (0.1mM final) and leupeptin (1mM final). After cell lysis, chromatin was sheared by sonication into 500 – 1000pb fragment (30sec ON/30sec OFF, 6 cycles, 4°C, Diagenode Bioruptor Pico). 10µl was kept aside as the input, and samples were divided in two halves, for minus and plus antibody treatment. FLAG-Tel1 immunoprecipitation was performed with 2µl of anti-FLAG antibody (M2 monoclonal, Sigma, Ref F1804) and incubation at 4°C for 2 hours. Pan-IgG mouse magnetic beads were incorporated for 2 more hours at 4°C. IP samples were washed by a 500mM NaCl containing lysis buffer and LiCl buffer (10mM Tris-HCl pH8, 0.25LiCl, 1mM EDTA pH8, 0.5% Triton X-100, 0.5% Sodium Deoxycholate). Chromatin was eluted from magnetic beads in elution buffer (TE 1X, 0.5% SDS) at 65°C for 10min. DNA-protein interaction was disrupted by incubation at 65°C overnight for IP and input samples. RNA was digested by RNAse A treatment (20µg total, 15min at 37°C) and proteins by proteinase K treatment (100µg total, 1hour at 42°C). DNA was purified on column (Qiagen DNA purification kit).

Quantitative PCR (qPCR) on ChIP samples

qPCR was performed on ChIP samples at a control site (within *CDC39*), DSB hotspots sites (*ARE1*, *ATF2*, *GAT1*) and axis sites (*YBP1*, *GRR1*) (see qPCR Primer Table) using the TB Green Premix Ex Taq II (Tli RNAse H Plus, Takara).

ChIP-seq

Tel1 and Spo11 ChIP-seq were performed following the ChIP-qPCR protocol with some modifications. For both FLAG-Tel1 and FLAG-Spo11 strain, cells were fixed in paraformaldehyde for 30min. Protein G magnetic beads were washed (0.1M NaHPO4 pH7.5, 0.01%Tween20, pH8.2) and saturated with BSA (0.1M NaP, 0.01% Tween20, 5mg/ml BSA) for 3hours at 4°C. Anti-FLAG antibodies (M2 Monoclonal, Sigma) were pre-incubated with saturated-magnetic beads for 4hours at 4°C. Cell lysis was performed as for the ChIP-qPCR protocol. Chromatin shearing was performed in Diagenode tube 15ml with beads (900 – 1000mg) by 7 cycles of sonication (30sec ON/30sec OFF, 4°C). Chromatin was immunoprecipitated with antibody-protein G mix by overnight incubation at 4°C. Samples were washed as for the ChIP-seq protocol, and DNA was eluted with IPure v2 Diagenode kit. DNA quantity was measured by QuBit and fragmentation quality was controlled by Agilent chip (Bio-analyser). DNA was sequenced with a NovaSeq sequencer (Illumina) using a 100nt paired-end protocol (TruSeq) at the Institut Curie sequencing facility (Paris, France).

Southern Blot

Genomic DNA was extracted from samples of synchronously sporulating cultures as described by Garcia et al 2011. Briefly, spheroplasts were prepared in 1M sorbitol, 0.1M EDTA, 0.1M NaHPO4 pH7.5, 1%BME and 200µg/ml zymolyase 100T for 30min at 37°C, and lysed by incubation with SDS (0.5% final) and proteinase K (200µg/ml final) for 1hour at 60°C. DNA was isolated from protein by adding equal amount of phenol:chloroform:isoamyl alcohol. DNA was precipitated by adding one-tenth volume of 3M sodium acetate pH5.2 and an equal volume of ethanol 100%. Precipitates were washed in 70% ethanol and resuspend overnight in TE 1X at 4°C. RNA was digested by RNAse A (100µg/ml final) for 60min at 37°C and DNA was reprecipitated with sodium acetate and ethanol before suspension in 1xTE buffer.
DSBs and double cuts were detected and measured as described in Garcia *et al*. 2015. Briefly, to measure meiotic DSBs, DNA was digested with the appropriate restriction enzyme (see Probe Table), whereas DCs were measured on undigested DNA. Digested and undigested DNA were fractioned in 0.7% agarose – TBE 1X gel for ~18h, transferred to nylon membrane under denaturing condition and hybridized with the appropriate probe for detection and quantification. DSB and DC level were quantified as described in Garcia et al, 2015 using the Fiji Software.

Pulse Field Gel Electrophoresis (PFGE)

DNA was prepared in plug as previously described (Gray et al 2013). Plugs were sealed in 1% agarose – 0.5X TBE gel, and chromosomes were fractioned using a CHEF-DRIII PFGE system (Bio-Rad) using the following program: 14°C; 6 V/cm; switch angle 120°; switch time of 30 – 30s for 3hours and time 3 – 6s for 20hours. DNA was transferred to nylon membrane under denaturing condition and hybridized with a *FRM2* probe (see Probe Table). DC level were quantified by Fiji Software.

Signal quantification and DSB interference

DSB interference values between DSB hotspots I and II at *HIS4::LEU2* were calculated as previously described (Garcia *et al.* 2015[1]). Briefly, double-cuts (DCobs, “observed” DC) were quantified using a central probe (*LEU2*) measuring double-cut frequency between the two hotspots. This signal was multiplied by three to take in account that this probe hybridises to three parental genomic locations (*HIS4::LEU2*, *leu2::hisG*, *nuc1::LEU2*). Expected double-cuts (DCexp) were calculated by multiplying the frequencies of DSBs measured at DSB I and II using a MRX2 probe. However, because of double-cut formation, the DSB II signal measured

using the *MRX2* probe is underestimated. To compensate for this loss, the DCobs signal was added to DSB II. DSB interference were calculated as followed: *1 – DCexp / DCobs*.

Western Blot

Protein were isolated by trichloroacetic acid (TCA) precipitation method. 10ml of sporulating cells were treated with 250µl of TCA10% and mechanically lysed by Fastprep agitation (4 cycles of 30sec at maximum agitation). TCA pellets were extracted from lysate, and dissolved in STE buffer (2% SDS, 0.5M Tris HCl pH8.1, 10mMEDTA, Bromophenol Blue) with heat at 90°C for 3min. After 10min of centrifugation at 16,000g 4°C, whole cell supernatant was transferred in new tubes and stored at -20°C.

Protein samples were loaded on a 6.5% SDS-polyacrylamide gel and blotted to 0.45µm nitrocellulose membrane. Membranes were saturated with 5% BSA – PBST. FLAG-Tel1 and Hsp104 were detected with an anti-FLAG mouse antibody (M2 monoclonal, Sigma, 1/3000) or anti-Hsp104 rabbit antibody (polyclonal, ab69549, abcam, 1/3000) respectively, and revealed with anti-mouse (Dako P0447, 1/5000) or anti-rabbit (Jackson Immuno Research 111-035-003, 1/5000) HRP conjugated secondary antibodies. Signal was detected using the HCL kit (ECL™ Primer Western Blotting Detection Reagent, Amersham™) and a Chemidoc system (Biorad). Signal were quantified with the ImageLab Software.

Data processing and computational analysis

Accession numbers

The ChIP-seq data generated in this study have been deposited at the Gene Expression Omnibus database.

Alignment and mapping

Sequencing quality control was determined using FastQC tool (http://www.bioinformatics.babraham.ac.uk/projects/fastqc/) and aggregated across samples using MultiQC. Reads with Phred quality score less than 30 were filtered out. For ChIP-seq, paired-end reads were mapped to Cer3H4L2 saccharomyces cerevisiae genome (PMID: 31649282) using *Bowtie2* (v2.3.4.3) (1) with default parameters. Only mapped reads were filtered in using *samtools view* (*--exclude-flags 4*) (2). Duplicate tags were removed using Picard Tools *MarkDuplicates* and mapped tags were processed for further analysis. For all subsequent analyses, mitochondrial genome, plasmid genome, and ribosomal DNA (rDNA) loci were blacklisted and removed. For visualization purpose, mapped tags were converted into BigWig and normalized by their library size using *bamCoverage* (--scaleFactor library_size_factor --binSize 5) (4). Here again, reads were extended using values previously computed by *bamPEFragmentSize* and used through the --extendReads option.

Wig files from Hop1, Rec8 and Red1 ChIP-seq data in the WT background were obtained from published study (PMID: 26258962; GSE69231) transformed in bedGraph file with *wig2bed* (BEDOPS v2.4.41) and converted into the Cer3H4L2 by adding 3078 bp from the position 65684 and 1173 bp bp from the position 95042 on the chrIII.

Spo11 ChIP-seq reads from GSE52863 (PMID: 24635992 - WT background; 3h, 4h and 5h after meiotic induction) and the matched input sequencing reads were aligned to the yeast Cer3H4L2 genome (PMID: 31649282) using *bowtie2* and duplicate sequencing reads were removed. BedGraph files for each time point were created using *bamCoverage* (--normalizeUsing RPKM -bs 10) (4) and subtracted from the input signal for subsequent analysis.

We used Integrative Genome Viewer (IGV) v2.9.4 (Thorvaldsdottir et al., 2013) for visualization of enrichment profiles (5). In Fig. 3a and b, FLAG-Tel1 and FLAG-Spo11 bigwig files correspond to merging between the two replicates, subtracting the input signal. Default set-up were used (windowing function = mean; type graph = bar chart) except scales which were adapted to visualise majority of peaks.

correlation between biological replicates
The degree of correlation between biological replicates was evaluated with a scatter plot and subsequent computation of Pearson's correlation coefficient (R^2) and Spearman's rank correlation coefficient (ρ) using the average signals in individual 100-bp non-overlapping genomic windows.

Hyper-ChIPable regions
The three negative control from FLAG-Tel1 sae2Δ, FLAF-Spo11 sae2Δ and sae2Δ strain (see fig S3a, left panel) were analyzed with the Macs2 software (3) to call ChIP-seq broad peaks, subsequently merged to create the blacklist of hyper-ChIPable regions (550 independent regions were found all over the genome).

Peak calling
To avoid forgetting any peaks and ensure greater precision in peak selection, Tel1 ChIP-seq binding sites, in the sae2Δ background, were determined with *Macs2 callpeak* (3) using 3 different p-value cut-off *(--bw 300 --nomodel --keep-dup 1 -p [0.05, 1e-2 and 1e-4])* and input reads as the control. NarrowPeak from duplicate samples were merged for the three p-value conditions and only the smaller region from overlapping peaks was considering (see fig S3a, right panel). For correlation analysis, we merged regions with distance <350bp and remove peaks of the FLAG-Tel1 sae2Δ t-0h peaks from the FLAG-Tel1 sae2Δ t-6h peaks list. Spo11 ChIP-seq binding sites, in the sae2Δ background, were determined with *Macs2 bdgbroadcall*. We remove peaks of the FLAG-Spo11 sae2Δ t-0h peaks from the FLAG-Spo11 sae2Δ t-6h peaks list. Red1, Hop1 and Rec8 ChIP-seq binding sites in the WT background were determined with *Macs2 bdgbroadcall* (-c 1.301 -l 100 -g 100). Axis sites were obtained by cross-referencing Red1, Hop1 and Rec8 binding sites at 1 bp minimum, considering sites that overlap at least two out of the 3 proteins binding sites.
For all peak calls described above, positions that overlap a hyper-ChIPable regions have been removed from the overlapping peak coordinate. We retained peaks > 200bp at the end.

Read density maps
Read occurrence profiles were obtained by extracting 5 kb on each side of the center of DSBs or axis sites and counting the reads per 20-bp bins using *annotatePeaks.pl* (HOMER) (8). For heatmap, the regions were sorted according to their average density profile and generated using *TreeView* (9).

Chromosome profiles
Cer3H4L2 mapped tags were counted within 1000 bp bins (*beedtools makewindows -w 1000*) (7) throughout the genome using *featureCounts* (v1.6.4) (6). Signal values were then normalized by library size, smoothened by applying Hann function with different window sizes (2.5, 5, 10,25 and 50kb), and displayed using homemade R scripts.

Centrome/telomere plot profiles
Cer3H4L2 mapped tags were counted across 1000bp binned (*beedtools makewindows -w 1000*) genomic regions using *featureCounts*. Signal values were normalized by library size, averaged according to their absolute distance to the feature of interest (e.g. centromere or telomere), and smoothened using ggplot2 (v3.1.1) (https://ggplot2.tidyverse.org) (*geom_smooth; method = 'loess'*).

Intersection between dataset
Intersection between each dataset were counted as the overlaps between axis, DSBs, Tel1 and Spo11 peaks at 1 bp minimum using *intersectBed* (7).
Each random set contained the same number of regions as in the cognate set of DSBs or Tel1 peaks and had the same length distribution, but each region segment was randomly picked with the condition that the segments did not overlap with any actual DSBs or Tel1 peaks (*shuffleBed* [-chrom -noOverlapping]) (7). The significance of the difference between random

(shuffled) and actual region (real) was derived from the distribution function of the normal distribution (data for random region were normally distributed, as verified with Shapiro–Wilk tests).
Venn diagrams were performed with *Venn Diagram Generator* (https://academo.org/demos/venn-diagram-generator/). Boxplot were generated *by GraphPad Prism v8.0.2* (GraphPad Software, Boston, Massachusetts USA, www.graphpad.com)

Statistics
For qPCR, statistical analysis was performed using two-way ANOVA multiple comparisons and Tukey's multiple-comparison test (alpha = 0.05); $*p \leq 0.05$, $**p \leq 0.01$, $***p \leq 0.001$ and $****p \leq 0.0001$. Error bars represent the mean ± SD of the indicated number of independent experiments.

REFERENCES
1. Langmead, B. and Salzberg, S.L. (2012) Fast gapped-read alignment with Bowtie 2. Nat Methods, 9, 357-359.
2. Li H.*, Handsaker B.*, Wysoker A., Fennell T., Ruan J., Homer N., Marth G., Abecasis G., Durbin R. and 1000 Genome Project Data Processing Subgroup (2009) The Sequence alignment/map (SAM) format and SAMtools. Bioinformatics, 25, 2078-9.
3. Zhang, Y., Liu, T., Meyer, C.A., Eeckhoute, J., Johnson, D.S., Bernstein, B.E., Nusbaum, C., Myers, R.M., Brown, M., Li, W. et al. (2008) Model-based analysis of ChIP-Seq (MACS). Genome Biol, 9, R137.
4. Ramirez, F., Ryan, D.P., Gruning, B., Bhardwaj, V., Kilpert, F., Richter, A.S., Heyne, S., Dundar, F. and Manke, T. (2016) deepTools2: a next generation web server for deep-sequencing data analysis. Nucleic Acids Res, 44, W160-165.
5. James T. Robinson, Helga Thorvaldsdóttir, Wendy Winckler, Mitchell Guttman, Eric S. Lander, Gad Getz, Jill P. Mesirov. Integrative Genomics Viewer. Nature Biotechnology 29, 24–26 (2011).
6. Liao, Y., Smyth, G.K. and Shi, W. (2014) featureCounts: an efficient general purpose program for assigning sequence reads to genomic features. Bioinformatics, 30, 923-930.
7. Quinlan, A.R. and Hall, I.M. (2010) BEDTools: a flexible suite of utilities for comparing genomic features. Bioinformatics, 26, 841-842.
8. Heinz S, Benner C, Spann N, Bertolino E et al. Simple Combinations of Lineage-Determining Transcription Factors Prime cis-Regulatory Elements Required for Macrophage and B Cell Identities. Mol Cell 2010 May 28;38(4):576-589. PMID: 20513432.
9. Saldanha AJ: Java Treeview--extensible visualization of microarray data. Bioinformatics. 2004;20(17):3246–3248. 10.1093/bioinformatics/bth349.

Figure 1

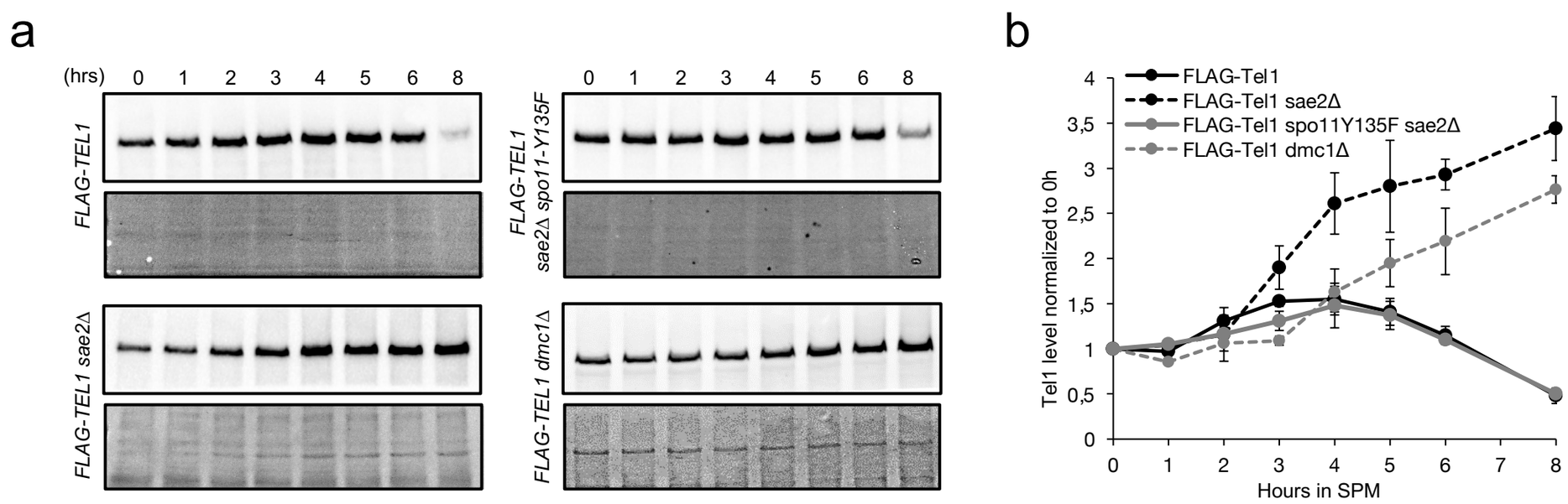
a
(hrs)
0 1 2 3 4 5 6 8
FLAG-TEL1
FLAG-TEL1 sae2Δ
FLAG-TEL1 sae2Δ spo11-Y135F
FLAG-TEL1 dmc1Δ
b
FLAG-Tel1
FLAG-Tel1 sae2Δ
FLAG-Tel1 spo11Y135F sae2Δ
FLAG-Tel1 dmc1Δ
Tel1 level normalized to 0h
0 0,5 1 1,5 2 2,5 3 3,5 4
0 1 2 3 4 5 6 7 8
Hours in SPM

Figure 2

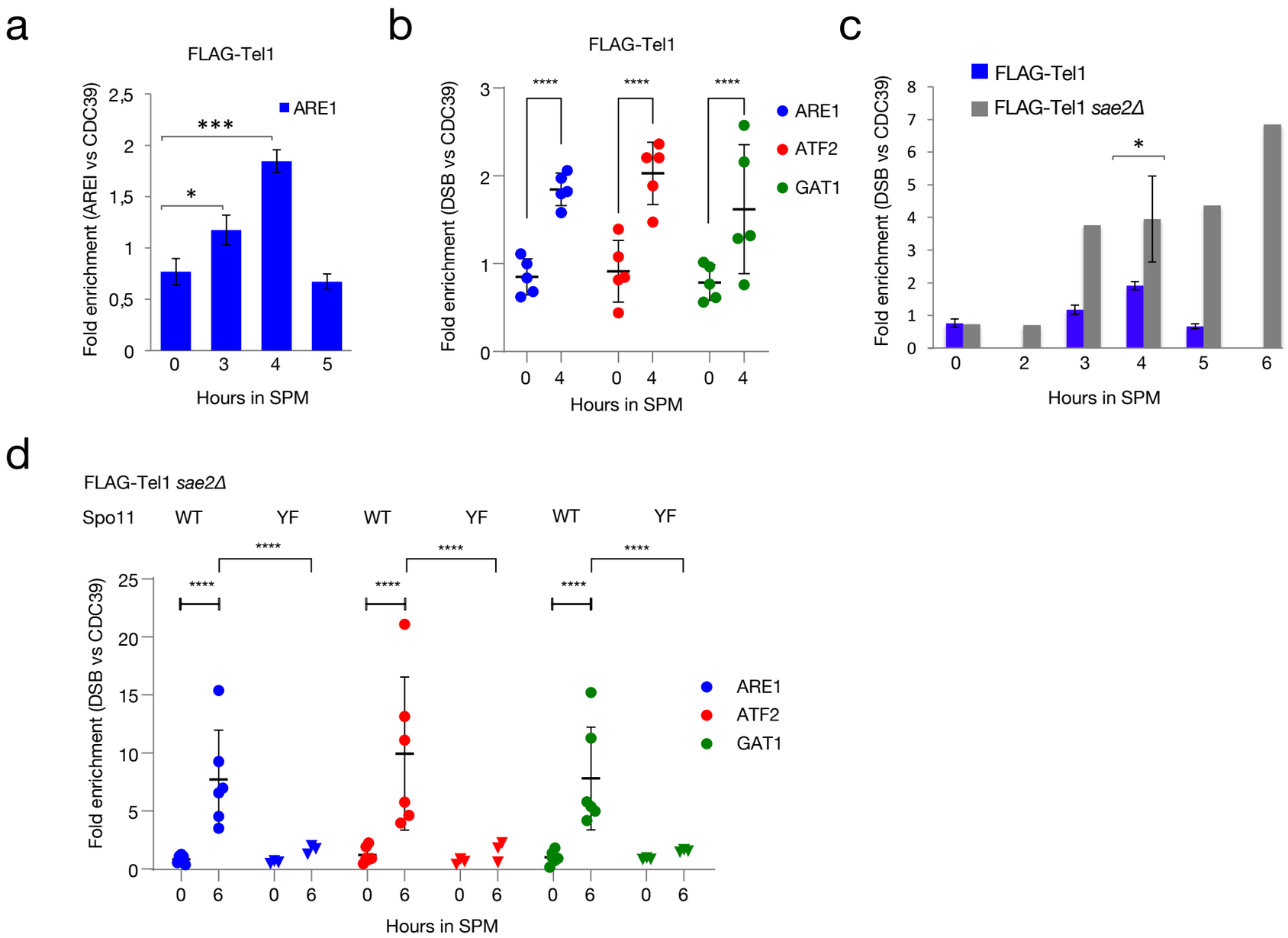
a
FLAG-Tel1
ARE1
Fold enrichment (AREI vs CDC39)
Hours in SPM
b
FLAG-Tel1
ARE1
ATF2
GAT1
Fold enrichment (DSB vs CDC39)
Hours in SPM
c
FLAG-Tel1
FLAG-Tel1 sae2Δ
Fold enrichment (DSB vs CDC39)
Hours in SPM
d
FLAG-Tel1 sae2Δ
Spo11
WT
YF
ARE1
ATF2
GAT1
Fold enrichment (DSB vs CDC39)
Hours in SPM

Figure 3

a

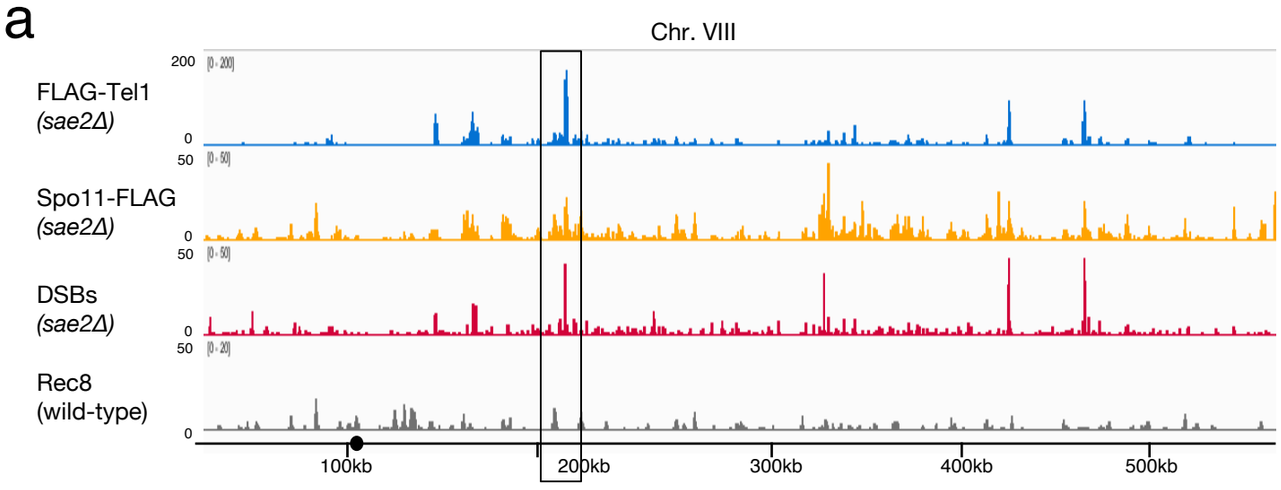

b

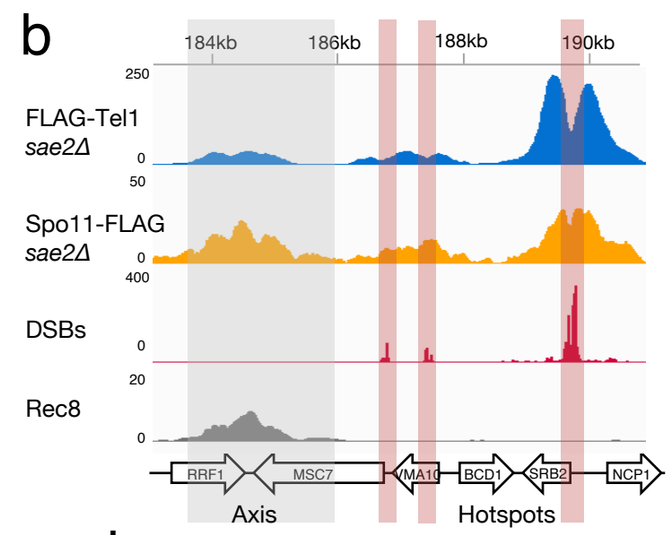

c

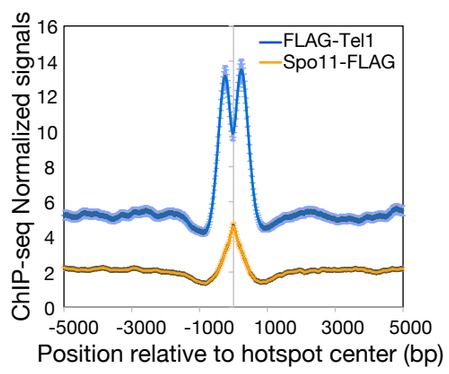

d

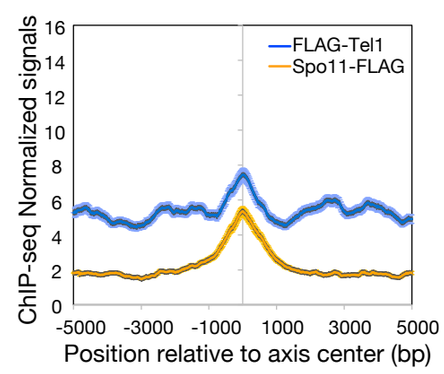

e

	Axis	DSBs	Tel1	Spo11
Axis	100%	22%	47%	47%
DSBs	39%	100%	59%	55%
Tel1	76%	60%	100%	70%
Spo11	87%	60%	81%	100%
alone	8%	25%	7%	16%

j

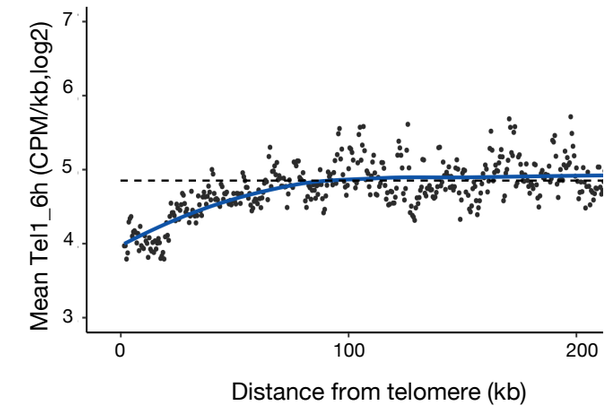

f

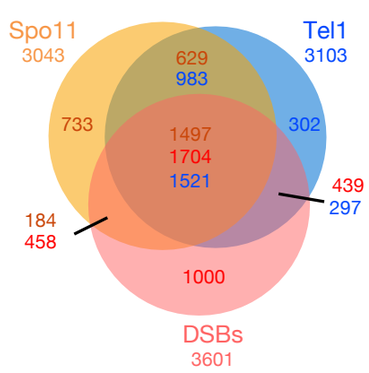

g

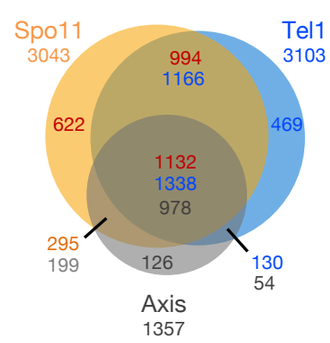

h

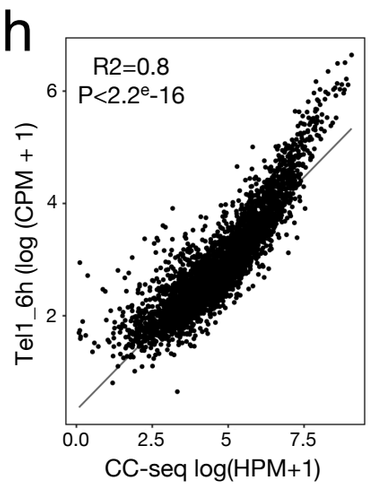

i

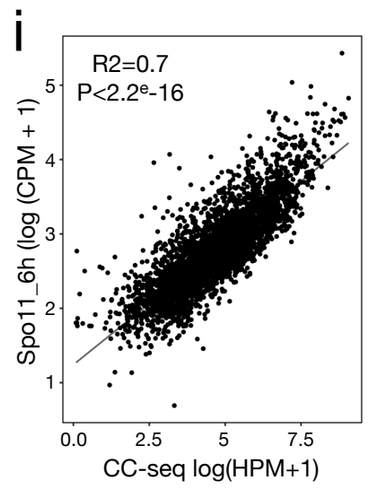

k

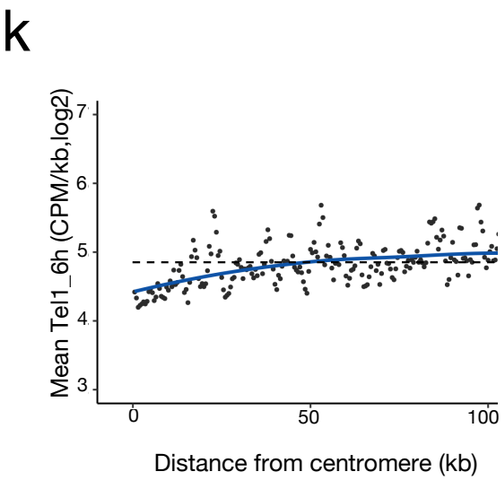

Figure 4

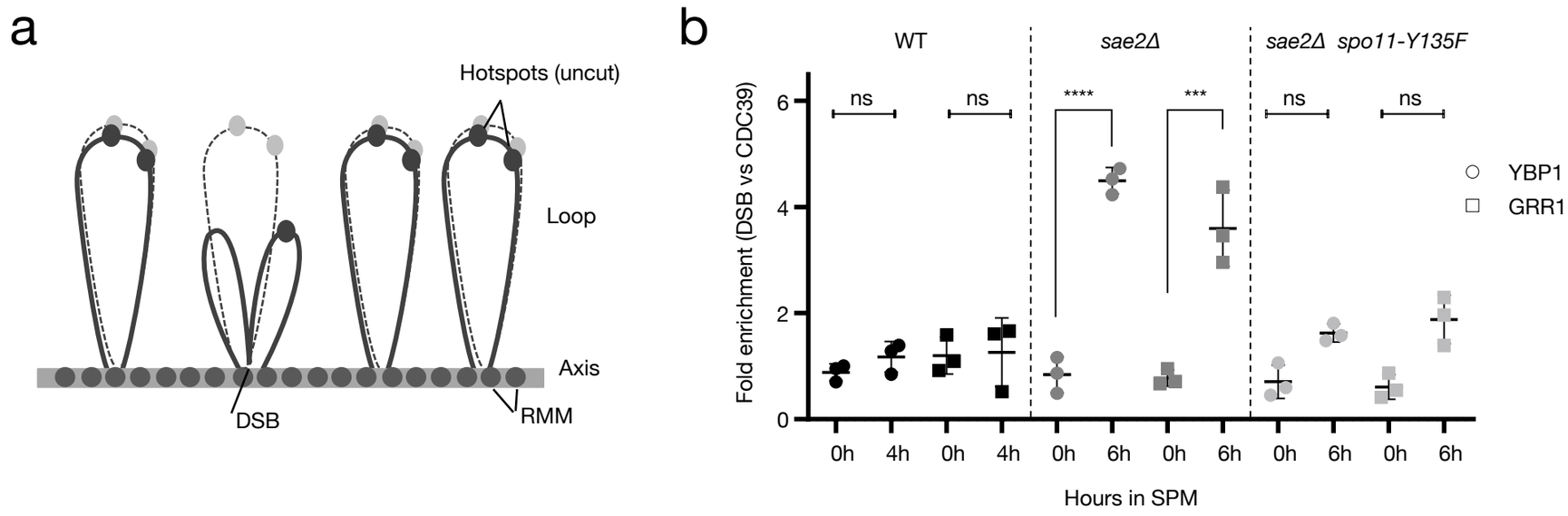
a
Hotspots (uncut)
Loop
Axis
DSB
RMM
b
WT
sae2Δ
sae2Δ spo11-Y135F
ns
ns
****
***
ns
ns
YBP1
GRR1
Fold enrichment (DSB vs CDC39)
0
2
4
6
0h
4h
0h
4h
0h
6h
0h
6h
0h
6h
0h
6h
Hours in SPM

Figure 5

a

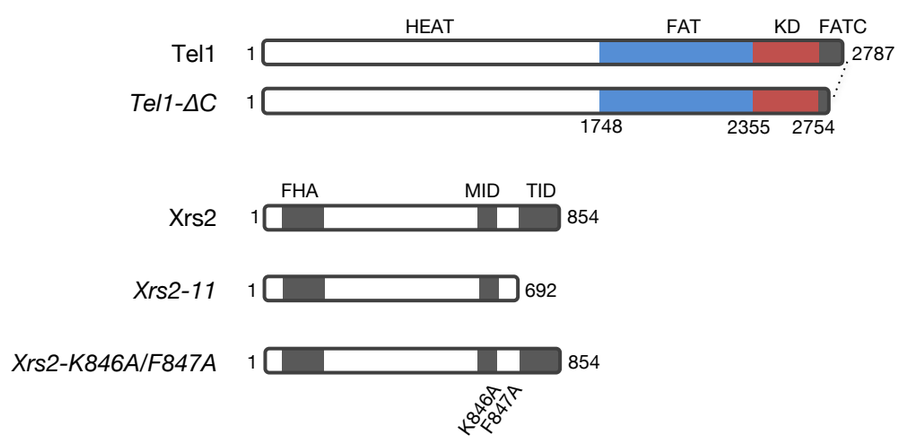
HEAT
FAT
KD
FATC
Tel1
1
2787
Tel1-ΔC
1
1748
2355
2754
FHA
MID
TID
Xrs2
1
854
Xrs2-11
1
692
Xrs2-K846A/F847A
1
854
K846A
F847A

b

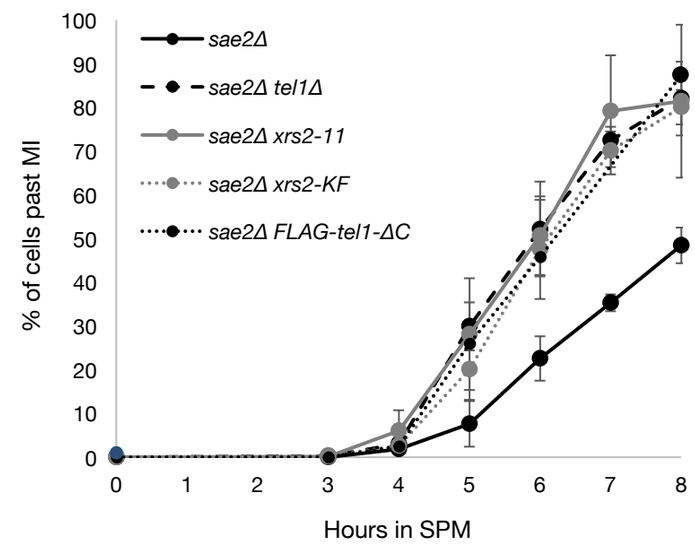
sae2Δ
sae2Δ tel1Δ
sae2Δ xrs2-11
sae2Δ xrs2-KF
sae2Δ FLAG-tel1-ΔC
% of cells past MI
Hours in SPM
0
10
20
30
40
50
60
70
80
90
100
0
1
2
3
4
5
6
7
8

c

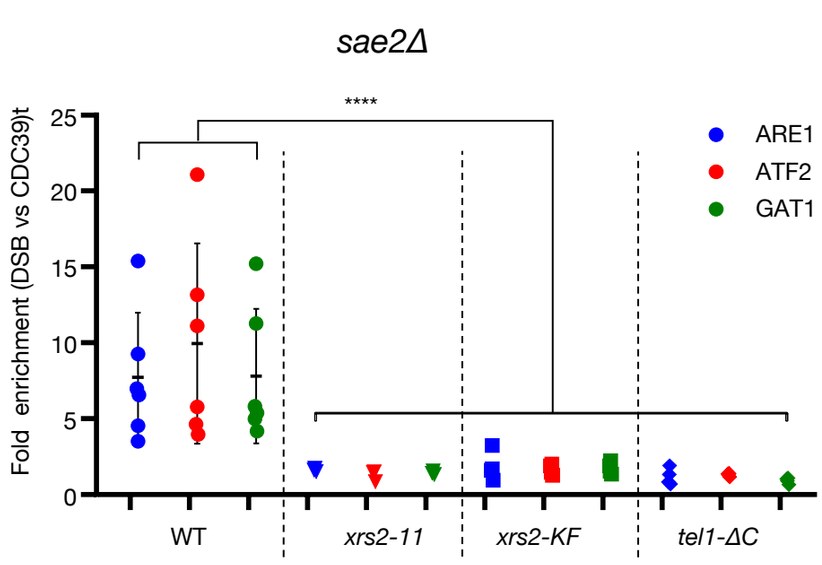
sae2Δ
****
ARE1
ATF2
GAT1
Fold enrichment (DSB vs CDC39)t
0
5
10
15
20
25
WT
xrs2-11
xrs2-KF
tel1-ΔC

Figure 6

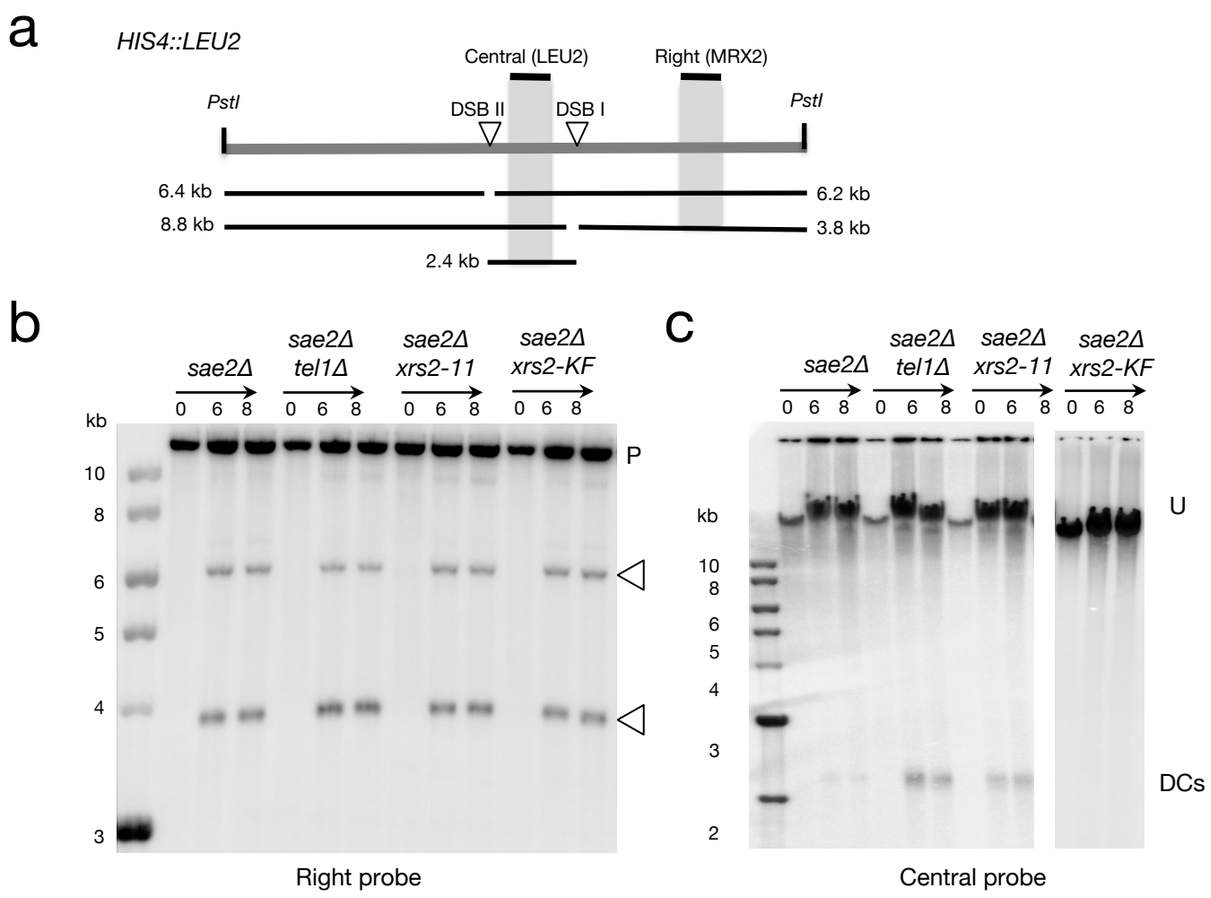
a
HIS4::LEU2
Central (LEU2)
Right (MRX2)
PstI
DSB II
DSB I
PstI
6.4 kb
6.2 kb
8.8 kb
3.8 kb
2.4 kb
b
sae2Δ
sae2Δ tel1Δ
sae2Δ xrs2-11
sae2Δ xrs2-KF
0 6 8
kb
10
8
6
5
4
3
P
Right probe
c
sae2Δ
sae2Δ tel1Δ
sae2Δ xrs2-11
sae2Δ xrs2-KF
0 6 8
kb
10
8
6
5
4
3
2
U
DCs
Central probe

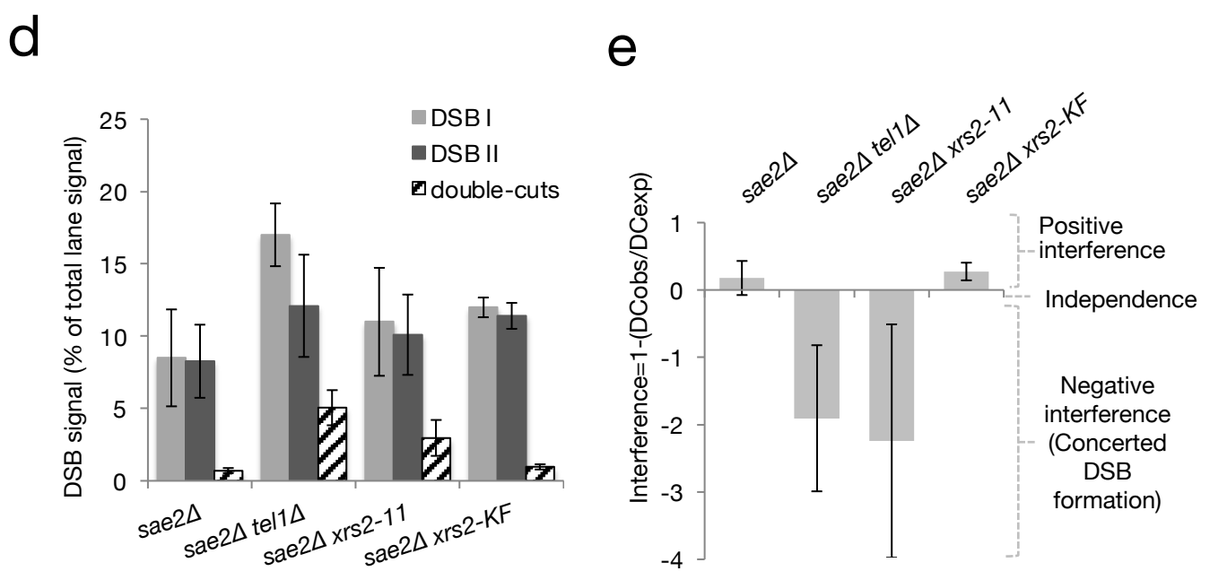
d
DSB I
DSB II
double-cuts
DSB signal (% of total lane signal)
25
20
15
10
5
0
sae2Δ
sae2Δ tel1Δ
sae2Δ xrs2-11
sae2Δ xrs2-KF
e
sae2Δ
sae2Δ tel1Δ
sae2Δ xrs2-11
sae2Δ xrs2-KF
Interference=1-(DCobs/DCexp)
1
0
-1
-2
-3
-4
Positive interference
Independence
Negative interference (Concerted DSB formation)

Figure S1

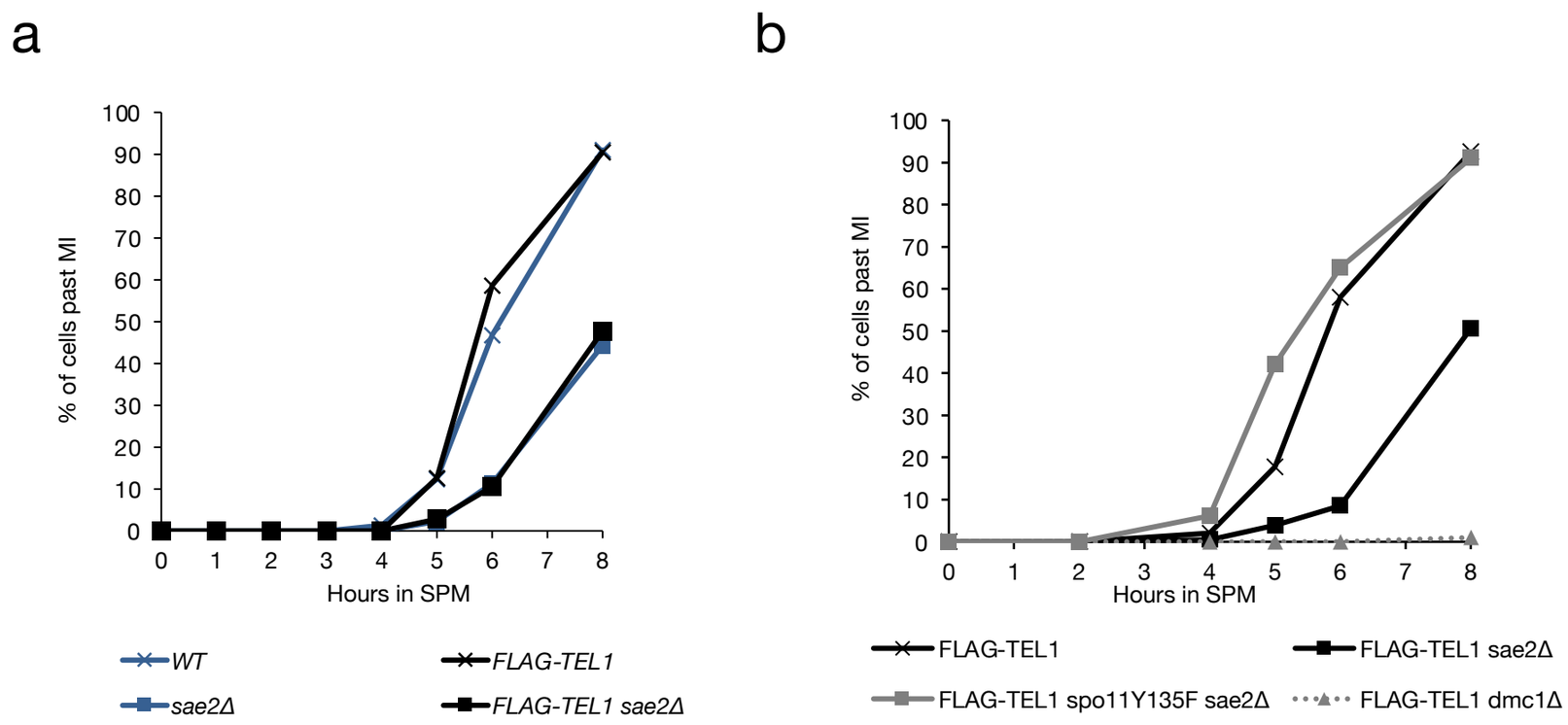
a
b
% of cells past MI
Hours in SPM
WT
sae2Δ
FLAG-TEL1
FLAG-TEL1 sae2Δ
FLAG-TEL1
FLAG-TEL1 sae2Δ
FLAG-TEL1 spo11Y135F sae2Δ
FLAG-TEL1 dmc1Δ

Figure S2

a

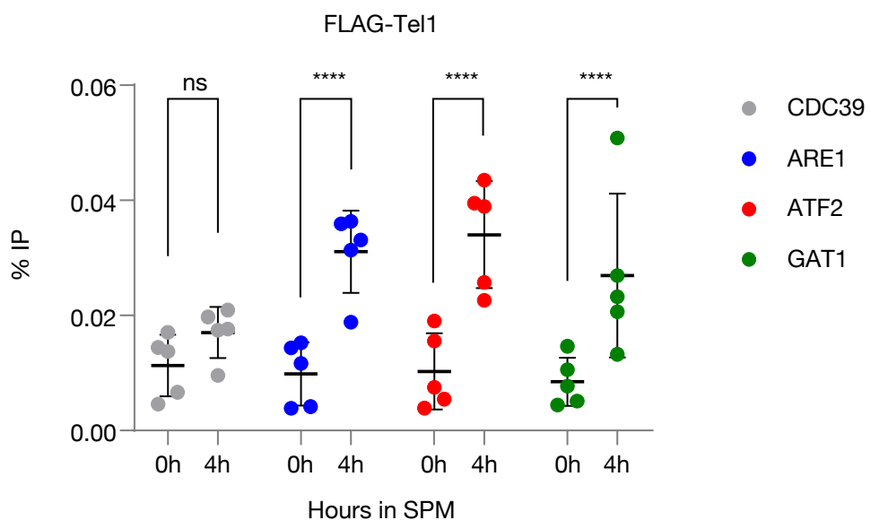

b

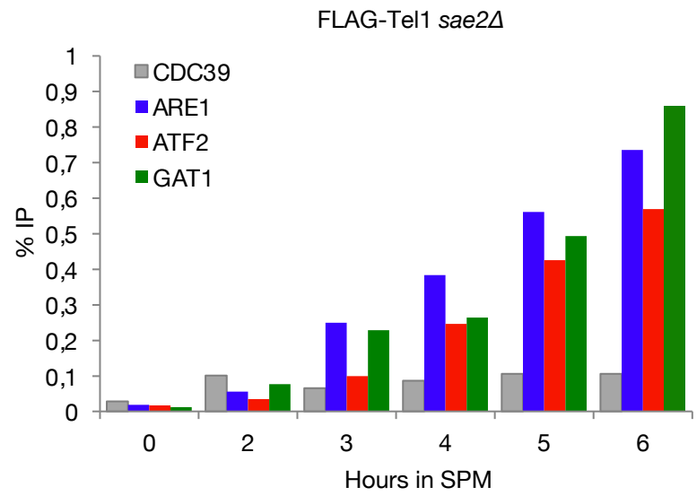

c

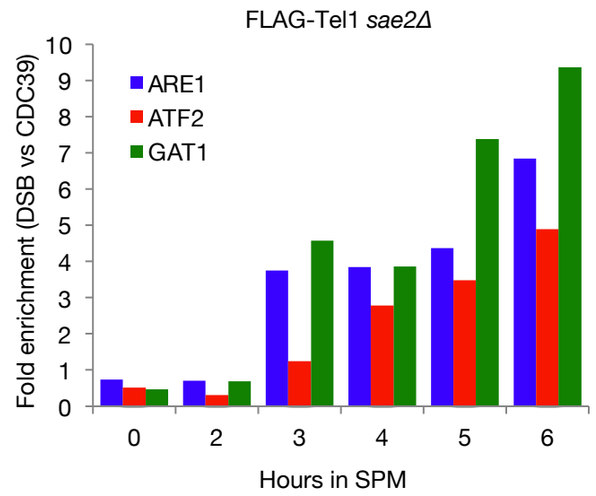

d

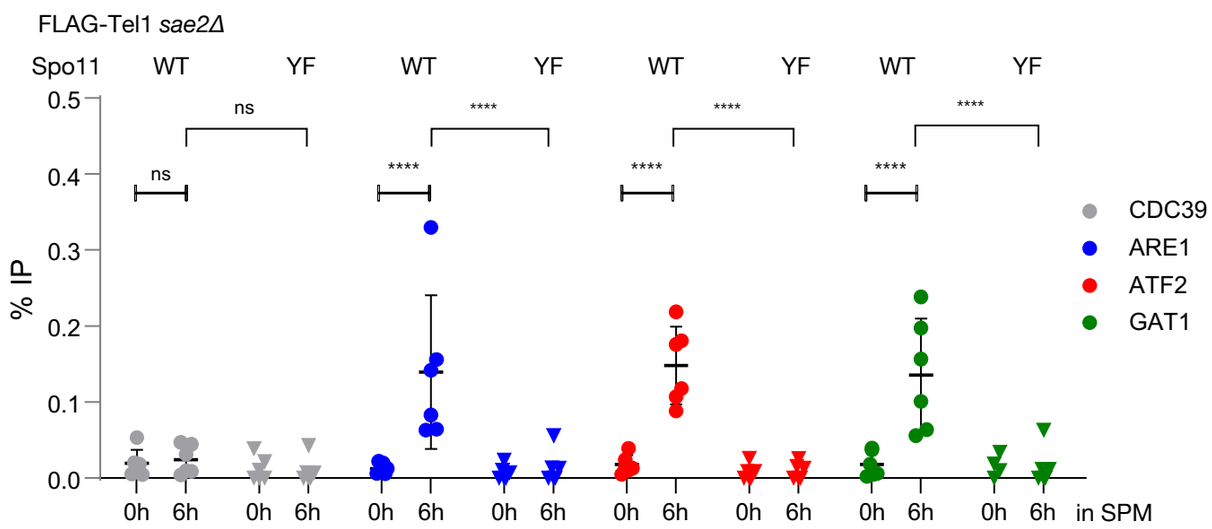

Figure S3

a

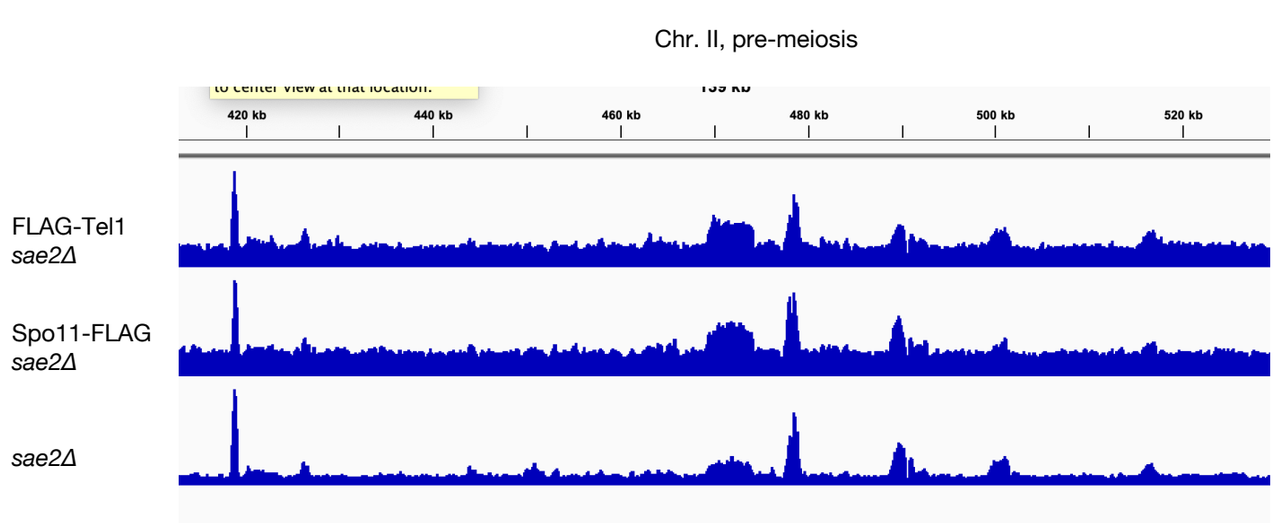
Chr. II, pre-meiosis
420 kb
440 kb
460 kb
480 kb
500 kb
520 kb
FLAG-Tel1
sae2Δ
Spo11-FLAG
sae2Δ
sae2Δ

b

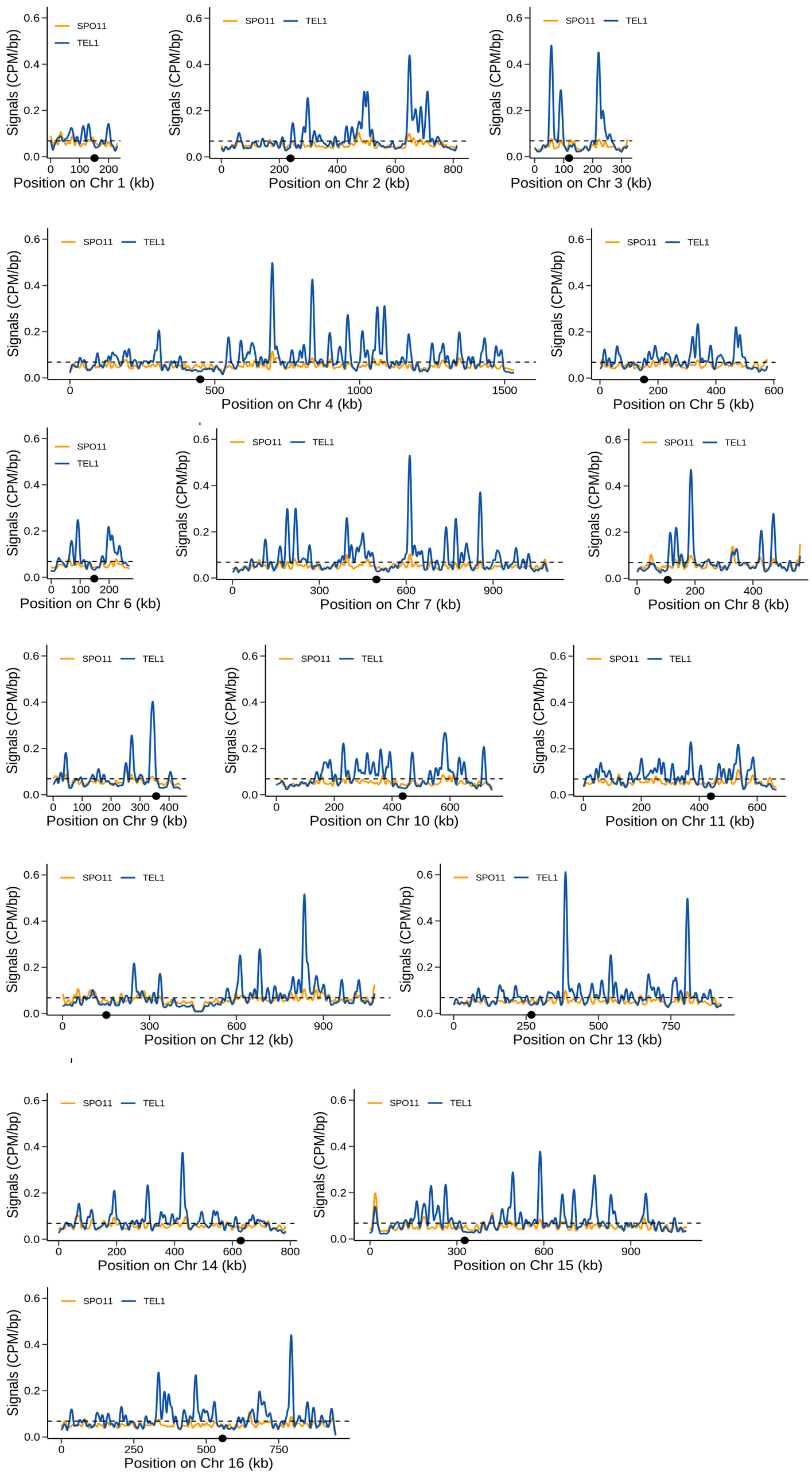
SPO11
TEL1
Signals (CPM/bp)
Position on Chr 1 (kb)
Position on Chr 2 (kb)
Position on Chr 3 (kb)
Position on Chr 4 (kb)
Position on Chr 5 (kb)
Position on Chr 6 (kb)
Position on Chr 7 (kb)
Position on Chr 8 (kb)
Position on Chr 9 (kb)
Position on Chr 10 (kb)
Position on Chr 11 (kb)
Position on Chr 12 (kb)
Position on Chr 13 (kb)
Position on Chr 14 (kb)
Position on Chr 15 (kb)
Position on Chr 16 (kb)

Figure S4

a

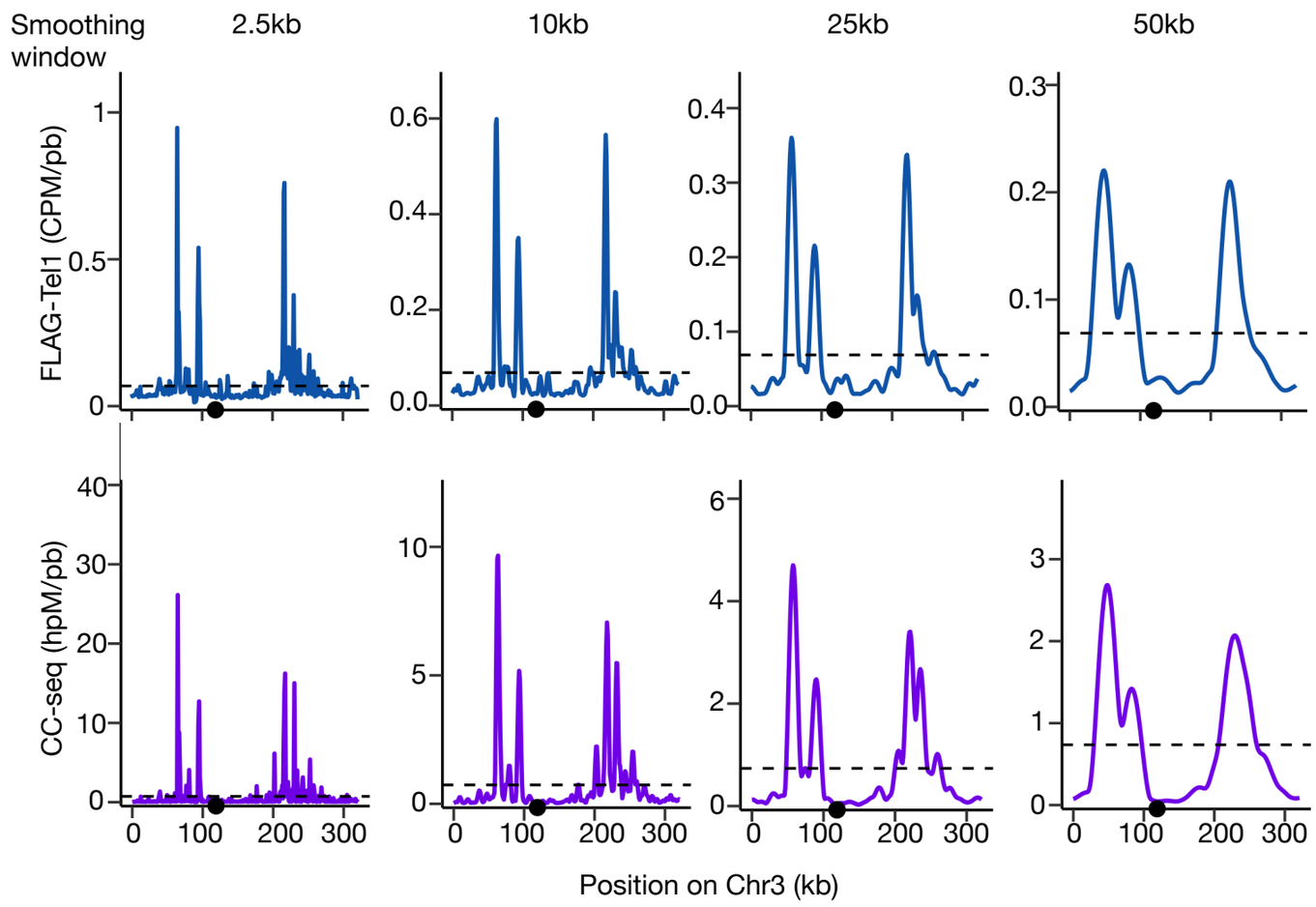
Smoothing window
2.5kb
10kb
25kb
50kb
FLAG-Tel1 (CPM/pb)
CC-seq (hpM/pb)
Position on Chr3 (kb)

b

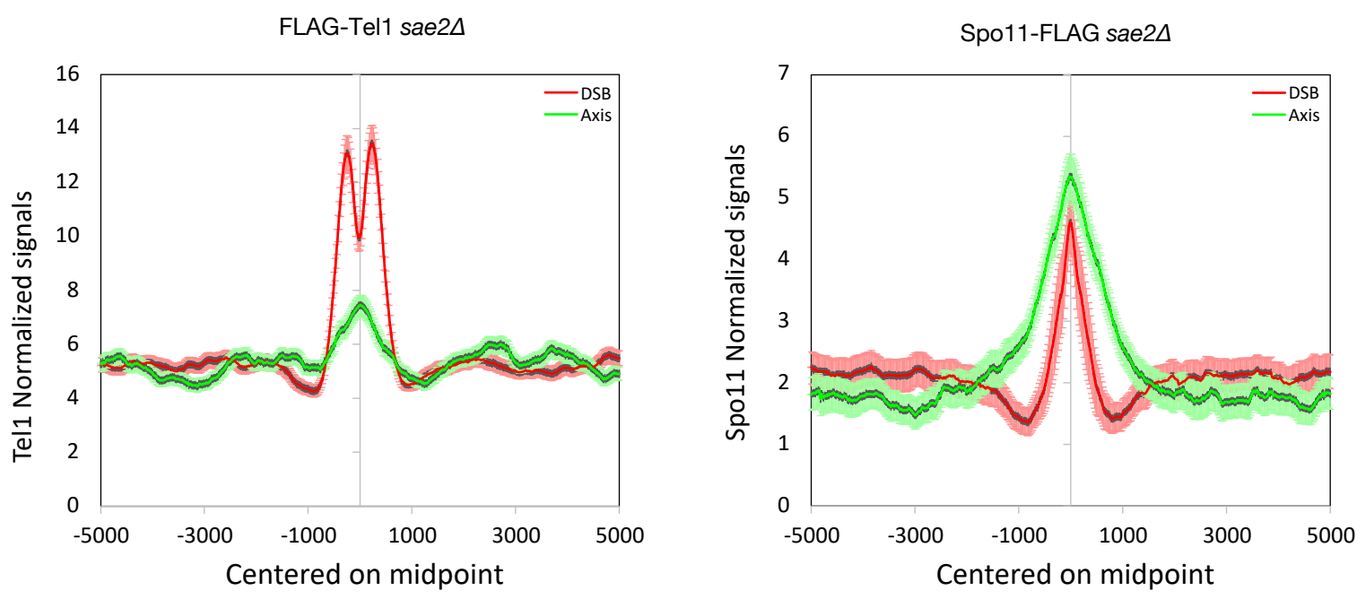
FLAG-Tel1 sae2Δ
Spo11-FLAG sae2Δ
DSB
Axis
Tel1 Normalized signals
Spo11 Normalized signals
Centered on midpoint

Figure S5

a

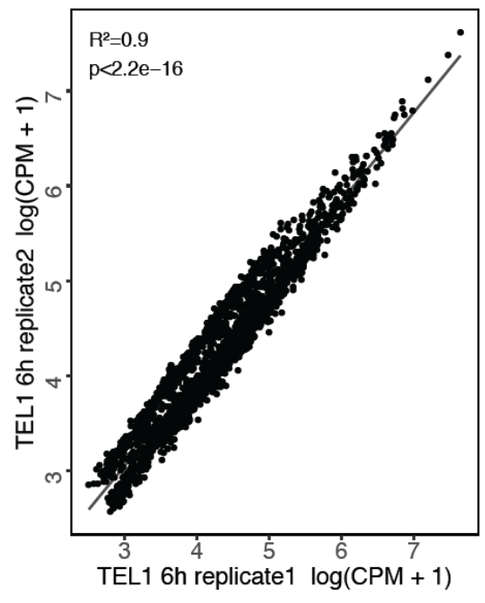

b

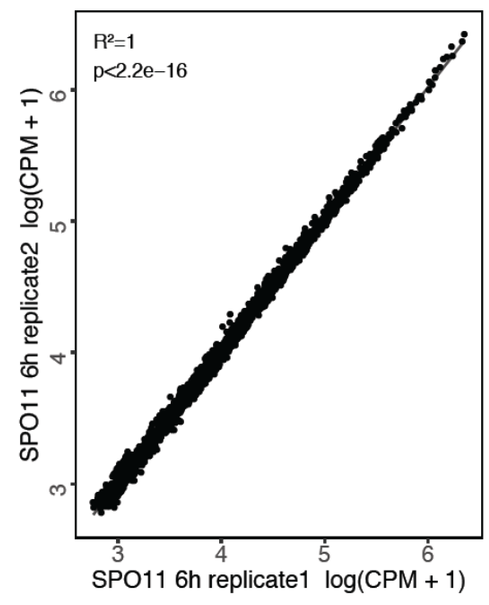

c

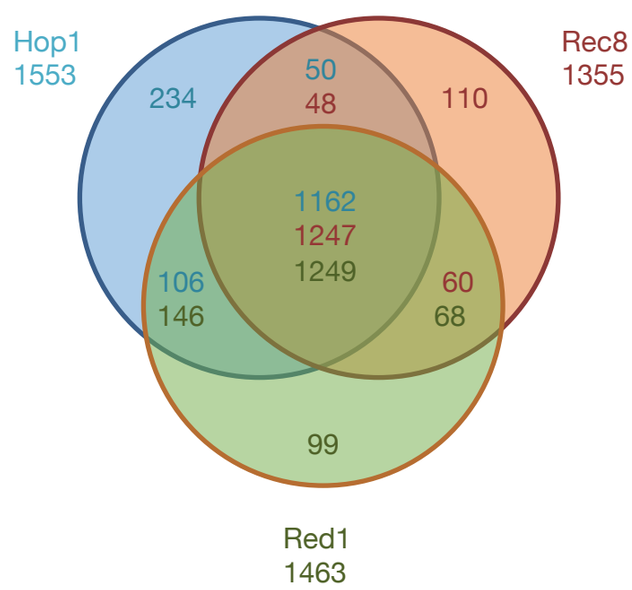

	UNIQUE	"Hop1" and "Rec8":	"Hop1" and "Red1":	"Rec8" and "Red1":	"Hop1", "Rec8" and "Red1":
Hop1	15.1%	3.2%	6.8%		74.9%
Rec8	7.5%	3.3%		4.1%	85.1%
Red1	6.3%		9.3%	4.4%	80.0%

d

	Axis	DSBs	Tel1	Spo11
Axis	1357	789	1468	1427
DSBs	535	3601	1818	1681
Tel1	1032	2143	3103	2126
Spo11	1177	2162	2504	3042
alone	114	910	230	489

e

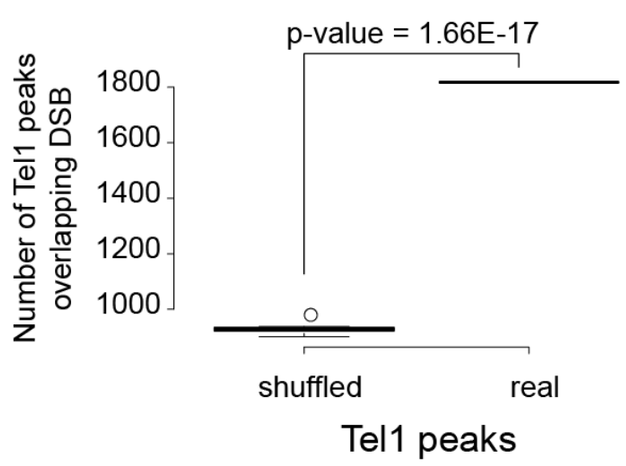

f

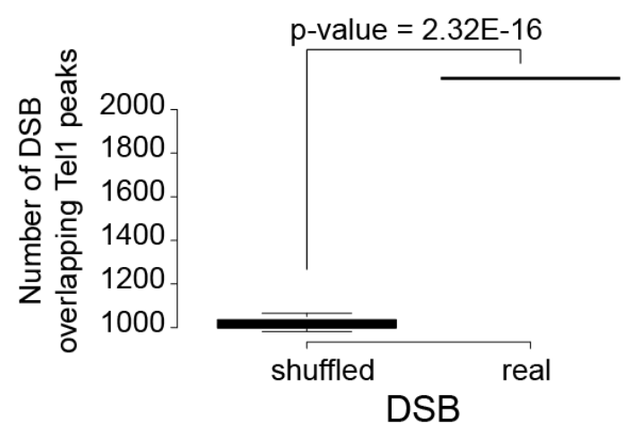

g

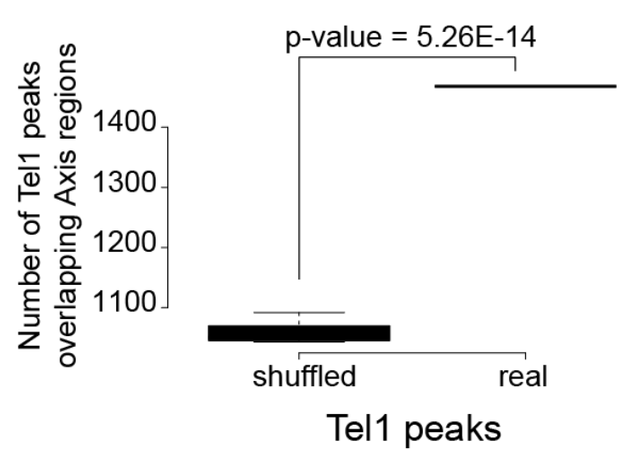

h

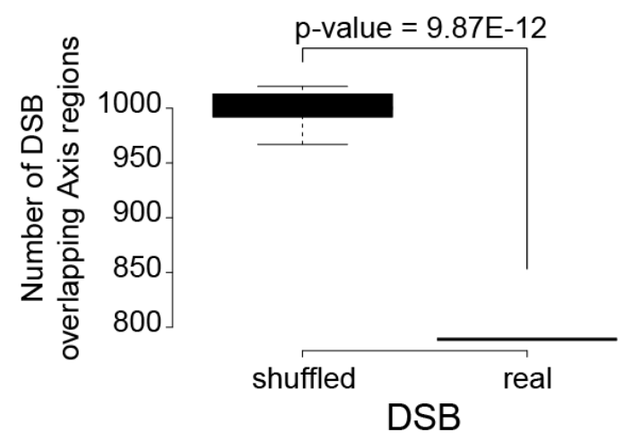

Figure S6

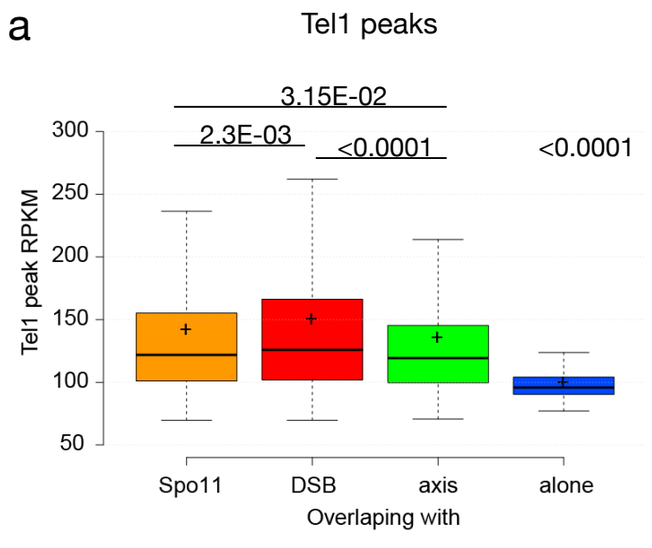
a
Tel1 peaks
3.15E-02
2.3E-03
<0.0001
<0.0001
Tel1 peak RPKM
300
250
200
150
100
50
Spo11
DSB
axis
alone
Overlaping with

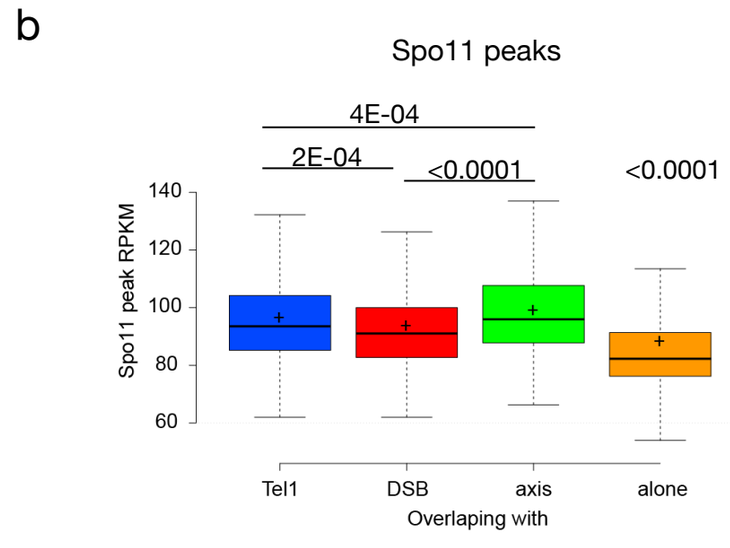
b
Spo11 peaks
4E-04
2E-04
<0.0001
<0.0001
Spo11 peak RPKM
140
120
100
80
60
Tel1
DSB
axis
alone
Overlaping with

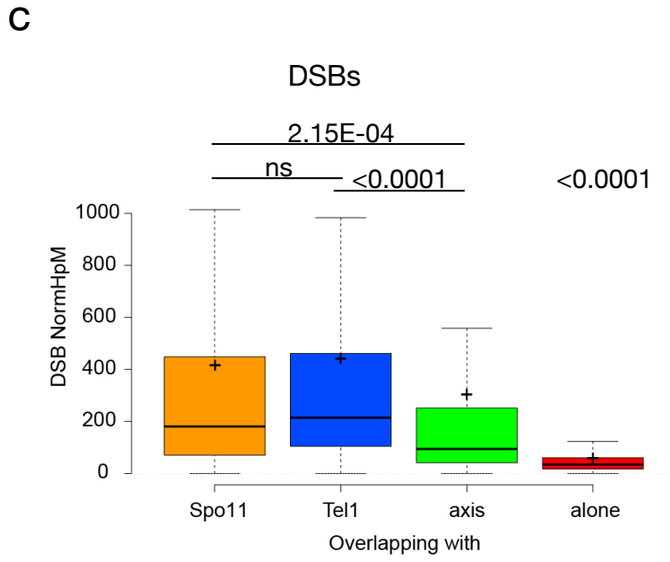
c
DSBs
2.15E-04
ns
<0.0001
<0.0001
DSB NormHpM
1000
800
600
400
200
0
Spo11
Tel1
axis
alone
Overlapping with

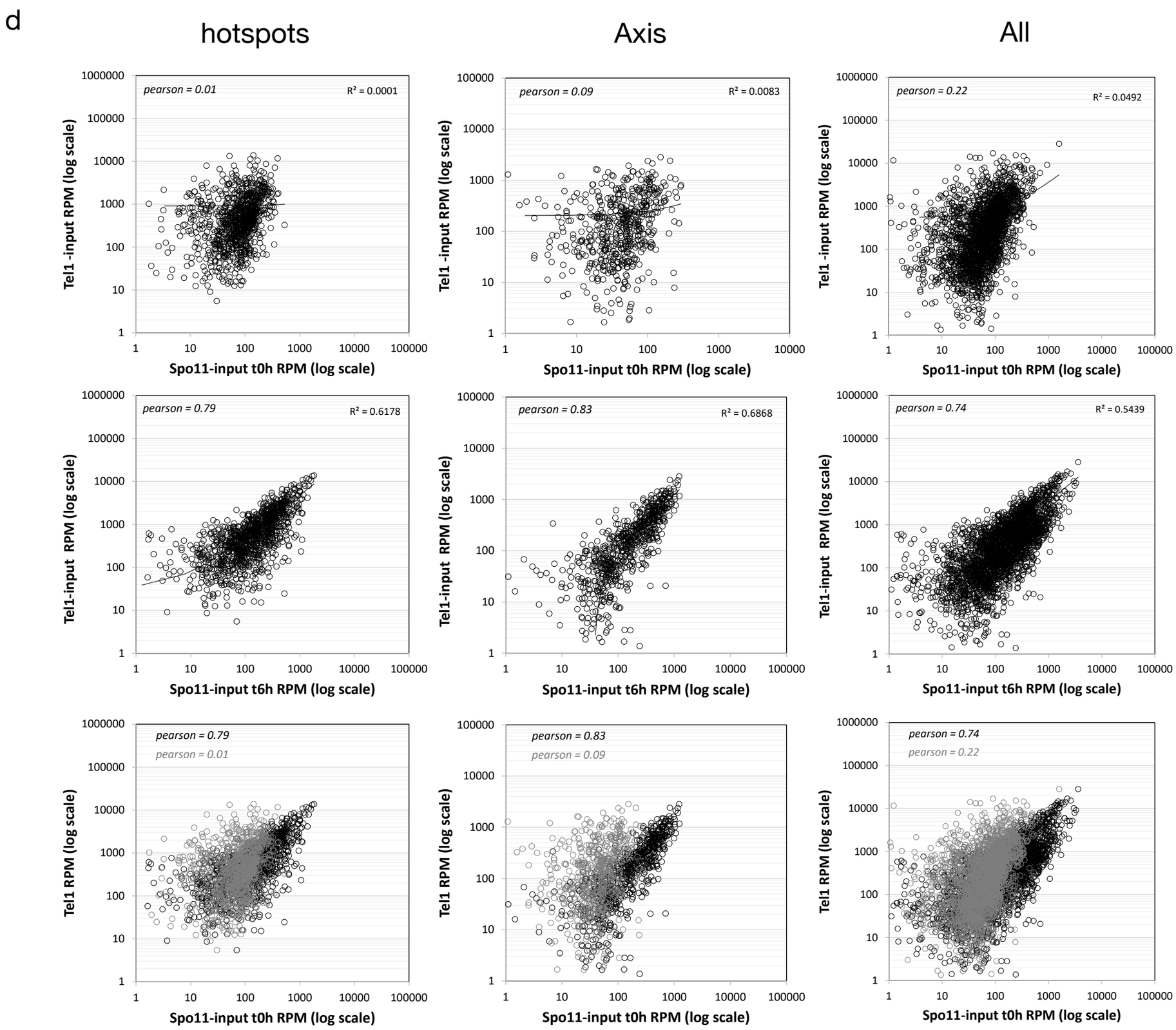
d
hotspots
Axis
All
pearson = 0.01
R² = 0.0001
pearson = 0.09
R² = 0.0083
pearson = 0.22
R² = 0.0492
pearson = 0.79
R² = 0.6178
pearson = 0.83
R² = 0.6868
pearson = 0.74
R² = 0.5439
pearson = 0.79
pearson = 0.01
pearson = 0.83
pearson = 0.09
pearson = 0.74
pearson = 0.22
Tel1 -input RPM (log scale)
Tel1-input RPM (log scale)
Tel1 RPM (log scale)
Spo11-input t0h RPM (log scale)
Spo11-input t6h RPM (log scale)
1
10
100
1000
10000
100000
1000000

Figure S7

a

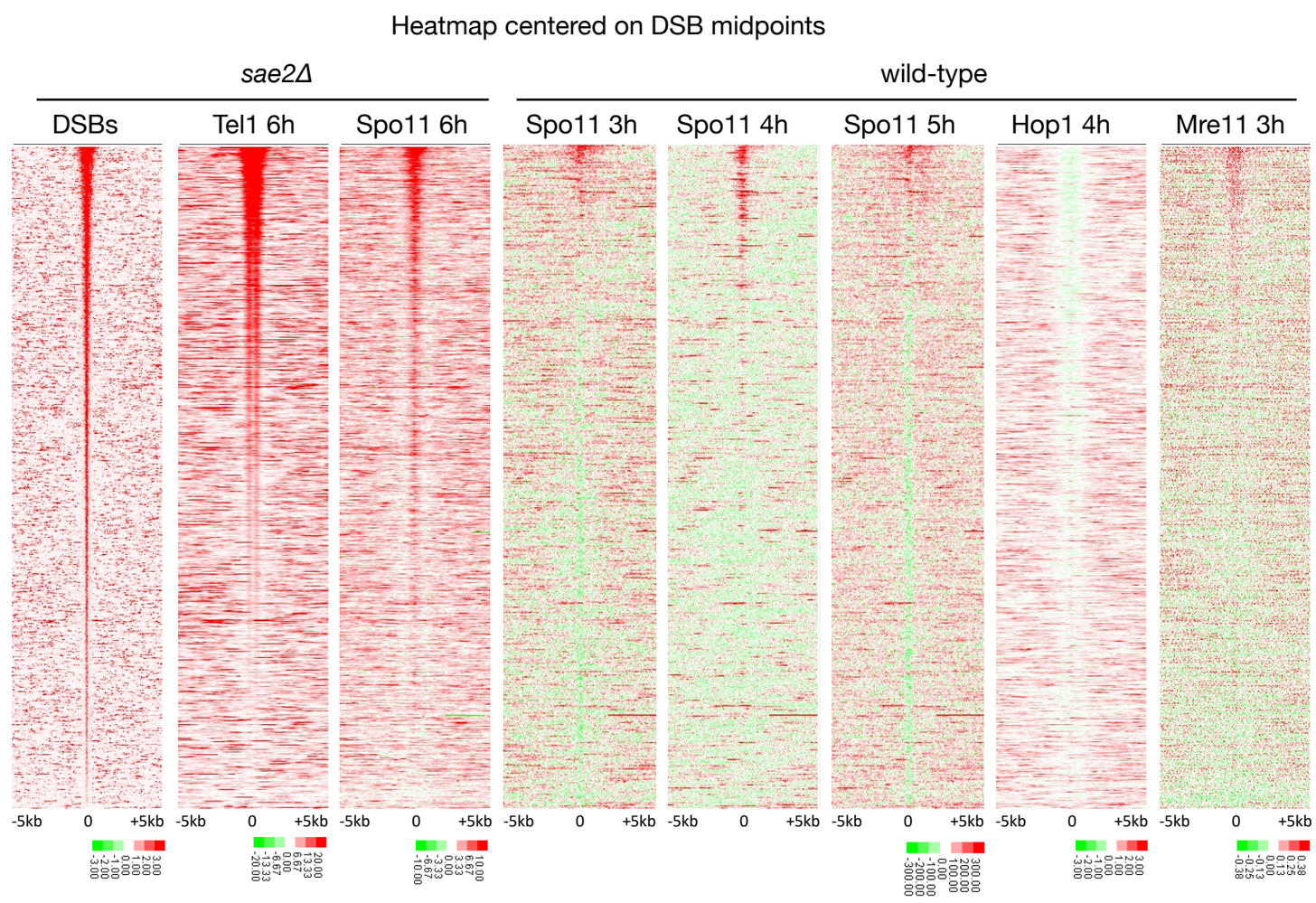
Heatmap centered on DSB midpoints
sae2Δ
wild-type
DSBs
Tel1 6h
Spo11 6h
Spo11 3h
Spo11 4h
Spo11 5h
Hop1 4h
Mre11 3h
-5kb
0
+5kb

b

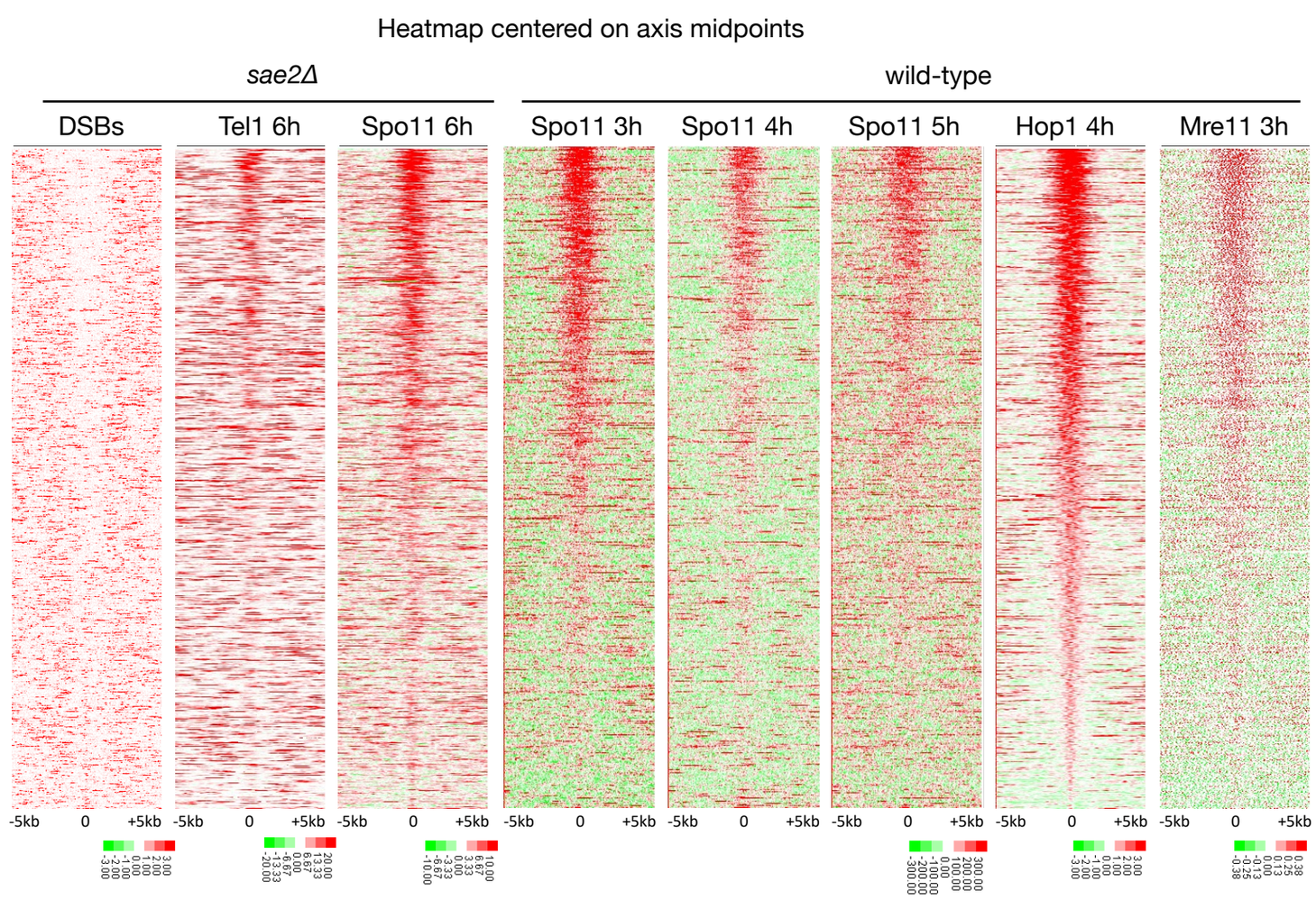
Heatmap centered on axis midpoints
sae2Δ
wild-type
DSBs
Tel1 6h
Spo11 6h
Spo11 3h
Spo11 4h
Spo11 5h
Hop1 4h
Mre11 3h
-5kb
0
+5kb

Figure S8

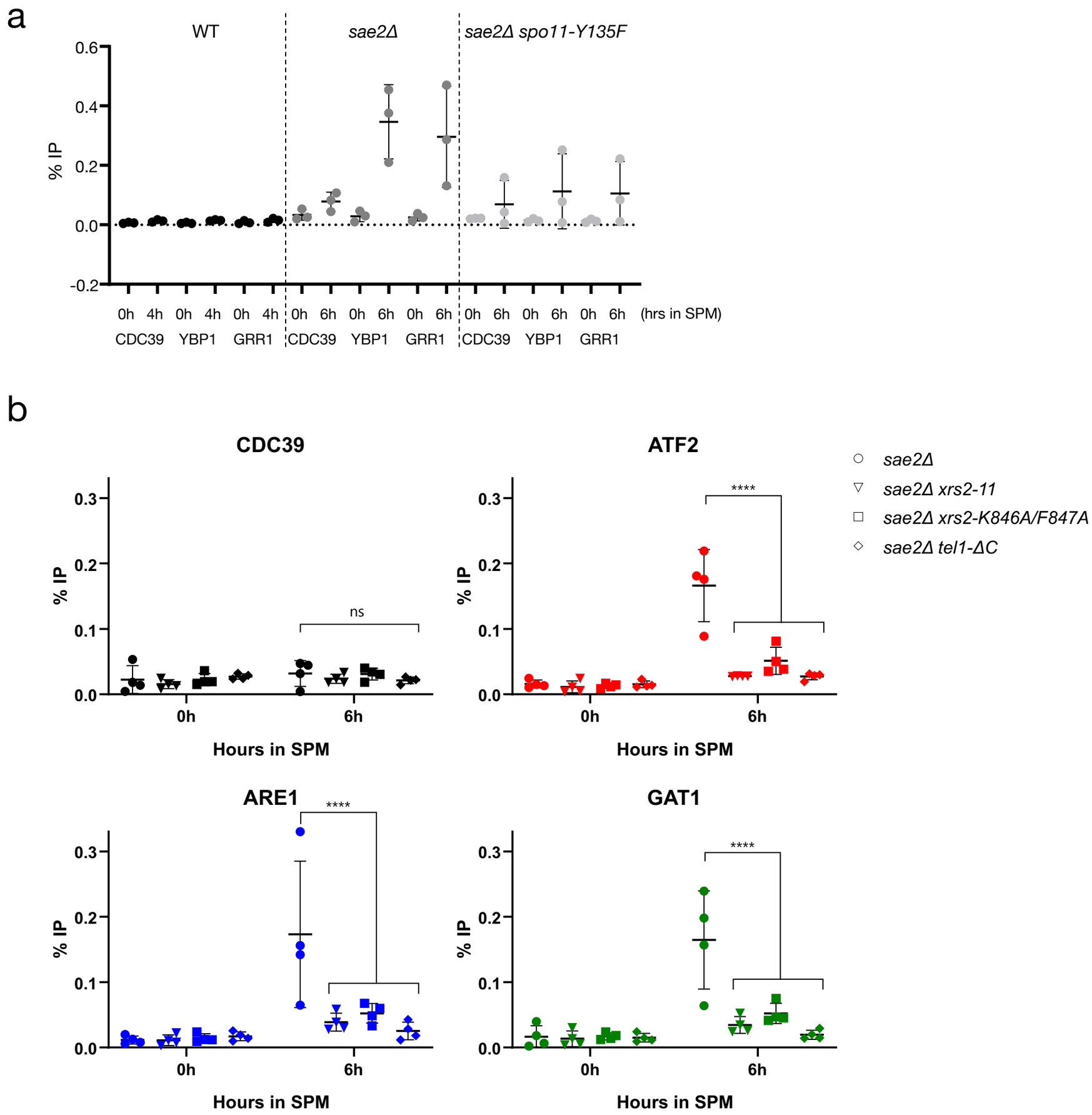
a
WT
sae2Δ
sae2Δ spo11-Y135F
% IP
0.6
0.4
0.2
0.0
-0.2
0h 4h 0h 4h 0h 4h 0h 6h 0h 6h 0h 6h 0h 6h 0h 6h 0h 6h (hrs in SPM)
CDC39 YBP1 GRR1 CDC39 YBP1 GRR1 CDC39 YBP1 GRR1
b
CDC39
ATF2
ARE1
GAT1
sae2Δ
sae2Δ xrs2-11
sae2Δ xrs2-K846A/F847A
sae2Δ tel1-ΔC
ns
****
% IP
0.3
0.2
0.1
0.0
0h
6h
Hours in SPM

Figure S9

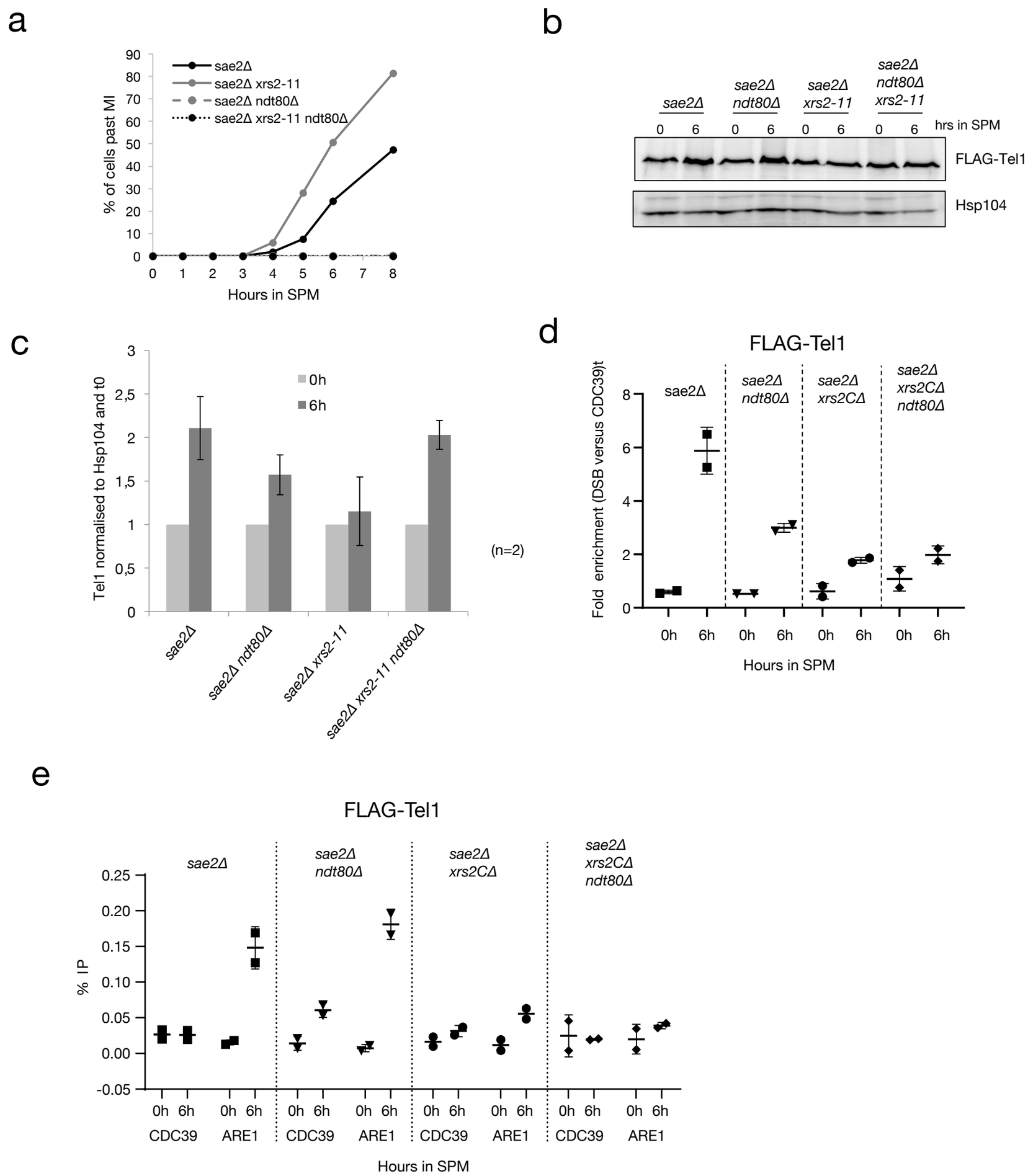
a
sae2Δ
sae2Δ xrs2-11
sae2Δ ndt80Δ
sae2Δ xrs2-11 ndt80Δ
% of cells past MI
Hours in SPM
b
sae2Δ
sae2Δ ndt80Δ
sae2Δ xrs2-11
sae2Δ ndt80Δ xrs2-11
hrs in SPM
FLAG-Tel1
Hsp104
c
0h
6h
Tel1 normalised to Hsp104 and t0
(n=2)
sae2Δ
sae2Δ ndt80Δ
sae2Δ xrs2-11
sae2Δ xrs2-11 ndt80Δ
d
FLAG-Tel1
sae2Δ xrs2CΔ ndt80Δ
Fold enrichment (DSB versus CDC39)t
Hours in SPM
e
FLAG-Tel1
% IP
CDC39
ARE1
Hours in SPM

Figure S10

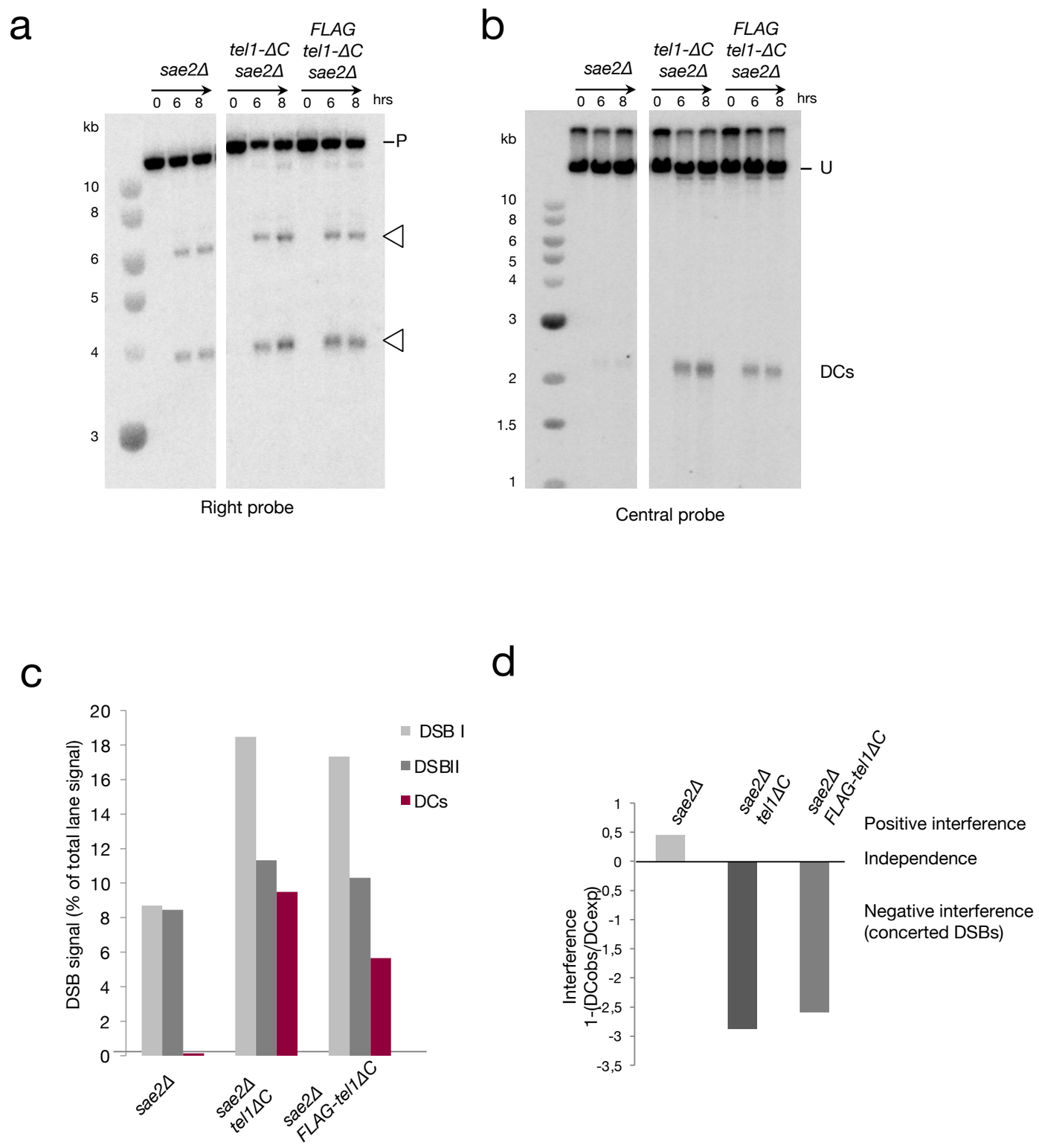
a
sae2Δ
tel1-ΔC sae2Δ
FLAG tel1-ΔC sae2Δ
0 6 8
0 6 8
0 6 8
hrs
kb
10
8
6
5
4
3
P
Right probe
b
sae2Δ
tel1-ΔC sae2Δ
FLAG tel1-ΔC sae2Δ
0 6 8
0 6 8
0 6 8
hrs
kb
10
8
6
5
4
3
2
1.5
1
U
DCs
Central probe
c
DSB signal (% of total lane signal)
20
18
16
14
12
10
8
6
4
2
0
DSB I
DSBII
DCs
sae2Δ
sae2Δ tel1ΔC
sae2Δ FLAG-tel1ΔC
d
Interference
1-(DCobs/DCexp)
1
0,5
0
-0,5
-1
-1,5
-2
-2,5
-3
-3,5
sae2Δ
sae2Δ tel1ΔC
sae2Δ FLAG-tel1ΔC
Positive interference
Independence
Negative interference
(concerted DSBs)

Figure S11

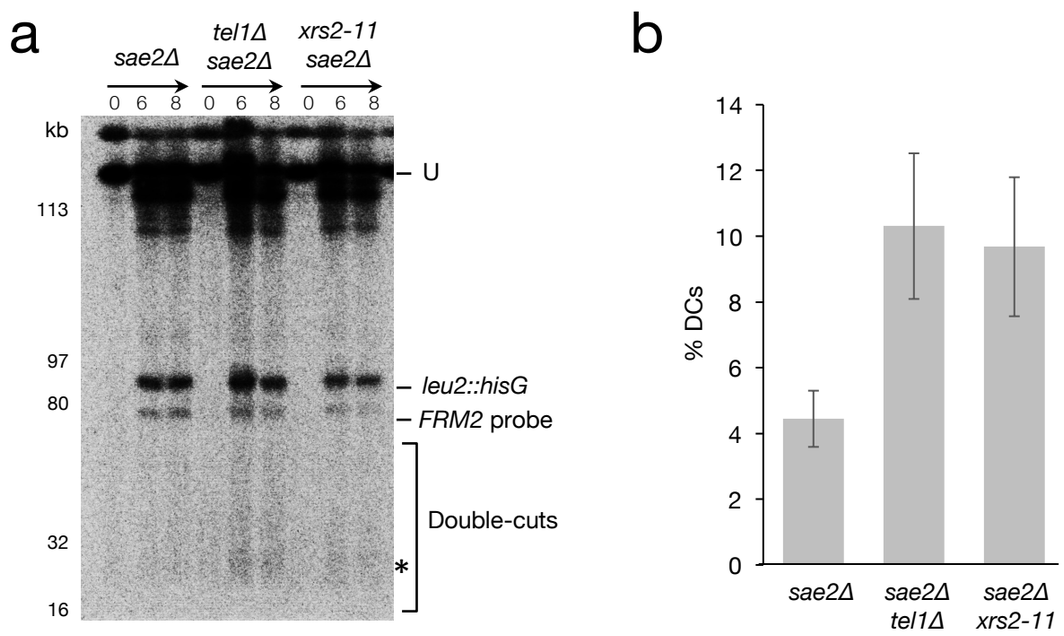
a
sae2Δ
tel1Δ sae2Δ
xrs2-11 sae2Δ
0 6 8 0 6 8 0 6 8
kb
113
97
80
32
16
U
leu2::hisG
FRM2 probe
Double-cuts
*
b
% DCs
14
12
10
8
6
4
2
0
sae2Δ
sae2Δ tel1Δ
sae2Δ xrs2-11

Table S1

Strain	Mating type	Genotype
VG499	a/α	*ho::LYS2/", lys2/", ura3/", arg4-nsp/", leu2::hisG/", his4X::LEU2/", nuc1::LEU2/", sae2Δ::KanMX6/"*
VG739	a/α	*ho::LYS2/", lys2/", ura3/", arg4-nsp/", leu2::hisG/", his4X::LEU2/", nuc1::LEU2/"*
VG740	a/α	*ho::LYS2/", lys2/", ura3/", arg4-nsp/", leu2::hisG/", his4X::LEU2/", nuc1::LEU2/", FLAG-TEL1", sae2Δ::KanMX6"*
VG741	a/α	*ho::LYS2/", lys2/", ura3/", arg4-nsp/", leu2::hisG/", his4X::LEU2/", nuc1::LEU2/", FLAG-TEL1"*
VG906	a/α	*ho::LYS2/", lys2/", ura3/", arg4-nsp/3, leu2::hisG/", nuc1::LEU2, SPO11-His6-flag3-loxP-HphMX-loxP/", sae2Δ::KanMX6/"*
VG613	a/α	*ho::LYS2/', lys2/', ura3/', arg4-nsp/', leu2::hisG/', his4X::LEU2/', nuc1::LEU2/', xrs2CterΔ/", sae2Δ::KanMX6/"*
VG619	a/α	*ho::LYS2/', lys2/', ura3/', arg4-nsp/', leu2::hisG/', his4X::LEU2/', nuc1::LEU2/', xrs2 K846A/F847A::KANMX6/", sae2Δ::KanMX6/"*
VG749	a/α	*ho::LYS2/", lys2/", ura3/", arg4-nsp/", leu2::hisG/", his4X::LEU2/", nuc1::LEU2/", FLAG-TEL1/", spo11(Y135F)::KanMX4/", sae2Δ::KanMX6/"*
VG764	a/α	*ho::LYS2/", lys2/", ura3/", arg4-nsp/", leu2::hisG/", his4X::LEU2/", nuc1::LEU2/", FLAG-TEL1/", sae2Δ::KanMX6/", xrs2CterΔ::KanMX6/"*
VG838	a/α	*ho::LYS2/", lys2/", ura3/", arg4-nsp/", leu2::hisG/", his4X::LEU2/", nuc1::LEU2/", FLAG-TEL1/", sae2Δ::KanMX6/", xrs2 K846A/F847A::KANMX6/"*
VG825	a/α	*ho::LYS2/", lys2/", ura3/", arg4-nsp/", leu2::hisG/", his4X::LEU2/", nuc1::LEU2/", FLAGTEL1/", dmc1Δ::HphMX4/"*
VG948	a/α	*ho::LYS2/", lys2/", ura3/", arg4-nsp/", leu2::hisG/", his4X::LEU2/", nuc1::LEU2/", FLAG-tel1-ΔC::NatMX6/", sae2Δ::KanMX6/"*
VG1212	a/α	*ho::LYS2/', lys2/', ura3/', arg4-nsp/', leu2::hisG/', his4X::LEU2/', nuc1::LEU2/', FLAG-TEL1/', sae2Δ::KanMX6/', xrs2CterΔ::KanMX6/', ndt80::HphMX/'*
VG1238	a/α	*ho::LYS2/", lys2/", ura3/", arg4-nsp/", leu2::hisG/", his4X::LEU2/", nuc1::LEU2/", FLAG-TEL1/", sae2Δ::KanMX6/", ndt80::HphMX/"*

Primers qPCR

Locus		Site	Forward Primer	Reverse Primer	Fragment size
CDC39	ChrIII	Control	CDC39_F@+3863 CGCTCCACCGATGACTCAAA	CDC39_R@+4014 CGACTGGGATGGCTGATTCA	151pb
ARE1	ChrIII	Hotspot	ARE1_F@-58 TCACGCAGGTGGTTGTTCAG	ARE1_R@+63 GGAATTGAGGCTGCGGATCTTA	121pb
ATF2	ChrVII	Hotspot	ATF2@F+1548 GAATGGGAATCGTTCTGCAAGC	ATF2@R+1671 CACTGCTTGCCTTTTGTACGAG	123pb
GAT1	ChrVI	Hotspot	GAT1@F+25 CGCCCTTCCCCTGTTCTG	GAT1@R+165 AAATTCAAGTCCGGGTCGAGG	138pb
YBP1	ChrII	Axis	YBP1_F@+1811 GGCAGATGCCAAGAAGAGTG	YBP1_R@+1962 CGGAAGTTTATCAGGTTCGACTG	151pb
GRR1	ChrX	Axis	GRR1_F@+3435 GCGTTCCTGATGCTTCATCC	GRR1_R@+3302 CCTGACCAGATGAGGAATCTCC	133pb

Primers probes Southern-blot

Probe		Forward Primer	Reverse Primer
MRX2	Chr III	HIS4_F@+5170 CGTGAAGTGGAACGATGCCC	HIS4_R@+5493 GCAACTGTTTCCAGCCTTCACC
LEU2	Chr III	LEU2_F ATATACCATTCTAATGTCTGC	LEU2_R AAGGATTTTCTTAACTTCTTCGGCG
FRM2	Chr III	FRM2_F@+27 GCTATTACAAACCGTCGTACCATC	FRM2_R@+645 CATCGCTGAGGTATCATTACTTCAT